Utrecht University
Faculty of Science

Master Degree in Nanomaterials Science

Characterizing (Sub)Nanometre Fluctuations in Biological and Bio-inspired Materials Using Optical Coherence Tomography

Nicola Mattiuzzo

Daily Supervisor: Pegah Asgari
First Examiner: Dr. Gerhard A. Blab
Second Examiner: Prof. Allard P. Mosk

Abstract

Optical coherence tomography (OCT) is a non-invasive imaging technique that generates high-resolution cross-sectional tissue images[1]. OCT is very common in ophthalmology and it is part of a group of techniques that are based on depth scans with low temporal coherence interferometry (LCI)[2].

However, the OCT technique can be widely used for different purposes. In this thesis with OCT we will be able to measure the thermal expansion of the polystyrene beads. Through the use of a laser and a broadband light source, we will target polystyrene microspheres (diameter 10 μm) doped with fluorophores. The laser hitting the microspheres will excite the fluorophores, which will release energy through heat and fluorescence.
The heat will cause the microsphere to expand and by using broadband light we will measure the difference in the optical path of light between the top and bottom surface of the microsphere to get thermal expansion.
The heat expansion will be analyzed for different laser powers in order to understand and verify the dilatation at different temperatures. In addition, a theoretical model will be developed to give explanations for the behaviour of the microspheres in relation to different laser powers used in the thesis.

Acknowledgments

To begin, I would like to thank my two supervisors; Dr. Gerhard Blab and Prof. Allard Mosk for their constant guidance in a project that differs from what was my prior knowledge and for giving me opportunities to learn new notions through this challenging project.
I would also like to thank Pegah Asgari for constantly supporting me throughout my thesis journey and having the patience to explain concepts previously unknown to me, and Itır Bakış Doğru-Yüksel for her support and advice.
I would like to thank all my classmates and the staff of the Nanophotonics research group for welcoming me and making me feel part of this university, without that it would have been difficult to undertake this task as an international student.
My thoughts and thanks also go to my Italian friends who, though distant, have always made their closeness felt.
The most important mention of thanks goes to my family: my grandparents, my father, my mother, my brother, my aunts, my cousins, and Gabriele and Nicola. They have been a tireless resource of strength during this time. This has been one of the most challenging experiences I have ever faced in my life, and they have always shown their belief in me. Without their love and support (financial and emotional) I would not be here now writing this master's thesis. I am eternally grateful to them. Their teachings have shaped me and I owe what I am today to them, and I will try in every way to repay them for what they have done for me.

Contents

Abstract **2**

Acknowledgments **3**

1 Introduction **6**

1.1 Microscopy 6

1.2 Confocal Microscopy 10

1.3 Fluorescence Microscopy 15

1.4 Optical Coherence Tomography 19

1.4.1 OCT techinques 22

2 Materials and Methods **25**

2.1 Experimental SetUp 25

2.2 Sample properties and preparation 27

2.3 Measurements 29

2.3.1 Expansion measurements 31

2.3.2 Control measurements 31

2.4 Analysis methods 32

3 Theoretical Model **35**

3.1 Heating model 35

3.2 OPL derivation 40

4 Results and Discussion **43**

4.1 Control measurements 44

4.2 Expansion measurements 49

4.3 Discussion 59

4.3.1 Discarded dataset 59

4.3.2 Beads' behaviors 62
4.3.3 Fresnel model 64

5 Conclusions **70**

Chapter 1

Introduction

1.1 Microscopy

Microscopy is the technical field of using microscopes to view samples and objects that cannot be seen with the unaided eye (objects that are not within the resolution range of the normal eye) [3].
Microscopes exploit the properties of light (such as reflection, interference etc.) to be able to draw as much information as possible from the sample.
Light is an electromagnetic wave that can be detected by the human eye[4]. Electromagnetic radiation is generated by changes in movement (vibration) of electrically charged particles, such as parts of 'heated' molecules, or electrons in atoms. Although classical physics had explained most of its behavior as a result of its undulatory nature, Planck and Einstein demonstrated that electromagnetic (EM) radiation behaves as if its energy were carried on a nanoscale in small bundles. Electromagnetic waves are emitted in the form of unitary packets, called photons. It is therefore not possible to emit the waves at an arbitrary rate. The photon is a minimum, indivisible quantity of energy that can be taken in discrete (not continuous) magnitudes by a physical quantity. It is a fundamental particle associated with interaction. The energy of the photon E is equal to Planck's constant (h) times the frequency of radiation (ν).

$$E = h \cdot \nu \tag{1.1}$$

Electromagnetic radiation extends from γ rays and X-rays through to radio waves and to the long radio waves[5]. The electromagnetic spectrum,

is the entire distribution of electromagnetic radiation according to frequency or wavelength. Although all electromagnetic waves travel at the speed of light in a vacuum, they do so with a wide range of frequencies, wavelengths and photon energies. The electromagnetic spectrum comprises the totality of all electromagnetic radiation and is composed of numerous subgroups, commonly called portions, such as visible light or ultraviolet radiation. The various portions bear different names based on the differences in behavior in the emission, transmission and absorption of the corresponding waves.

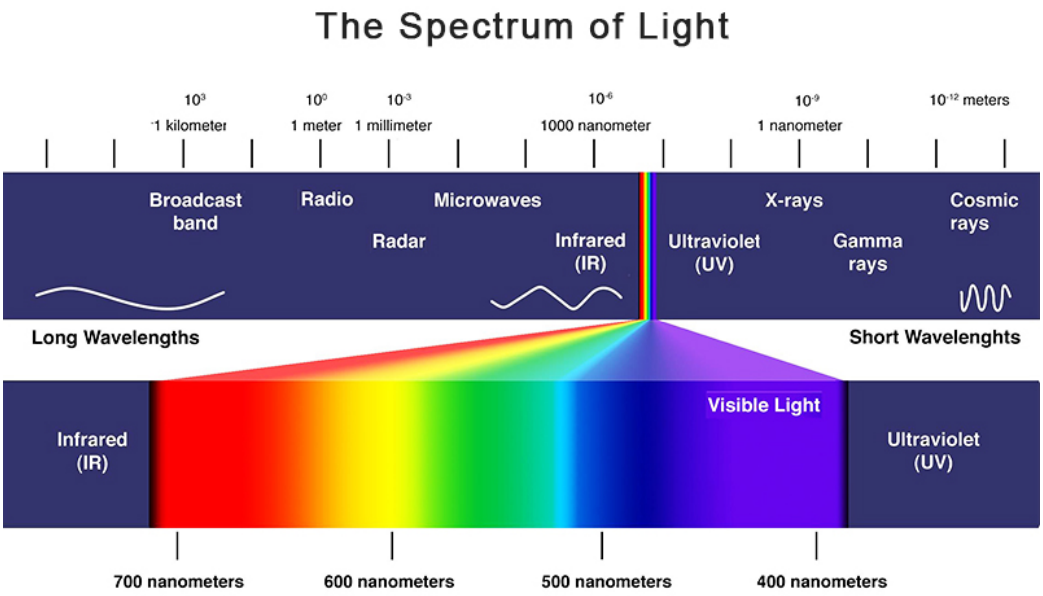

Figure 1.1: Spectrum of the light taken from Vanq[6].

Within this broad spectrum, the wavelengths visible to humans occupy a very narrow band, ranging from about 700 nanometers for red light to about 400 nanometers for violet light.
In the most common techniques of microscopy (wide field microscopy), light is totally transmitted toward the specimen, i.e. illuminated from below and observed from above. Basically, a microscope consists of two subsystems:

an illumination system to light the specimen and an imaging system where light generates a magnified image of the specimen that it has interacted with, which through camera systems can be observed with the human eye.

Currently, most microscopes use artificial light sources such as bulbs, light-emitting diodes (LEDs) or lasers to create more reliable and controllable illumination systems that can be tailored to a given application. In these systems, light from the source is typically collected by a condensing lens, optically patterned and filtered before being focused on the sample. Light shaping is essential to achieve high resolution and contrast[7].

One of the main goals of microscopy is to obtain images with good definition and resolution. Resolution is the shortest distance between two points visible to the eye, with or without the aid of a microscope[8]. Resolution is not a quantity that increases arbitrarily, but it is a factor that can be quantitatively calculated.

Ernst Abbe pioneered a quantitative analysis of the resolution limit of an optical microscope[9].In the case of an immersion microscope objective with circular aperture and direct on-axis illumination, the Abbe diffraction limit of resolution d reads

$$d = \frac{\lambda}{\mathrm{NA}} \tag{1.2}$$

where λ is the wavelength of the light and NA is the numerical aperture. The numerical aperture provides an indication of how much light can be collected and the resolution of the lens.

NA value increases as the number of photons collected increases, it is defined as:

$$\mathrm{NA} = n \cdot \sin\theta \tag{1.3}$$

Here, n is the refractive index of the medium and θ is the half-angle of the cone of the light that enters the objective.

Abbe's resolution criterion still finds use today, however, Rayleigh expanded

the concept of resolution to spectrometers and imaging instruments.

$$d = 1.22 \cdot \frac{\lambda}{2\mathrm{NA}} \tag{1.4}$$

It states that two close-lying points are considered resolved if the first intensity maximum of one diffraction pattern described by an Airy disc[10] coincides with the first intensity minimum of the other diffraction pattern[11].

Every measurement needs an observable, that is a signal. In optical microscopy, one correlates a certain optical signal from the sample with the spatial position of the signal source. Scattering is one of the origin of the signal or contrast mechanism in imaging[12].

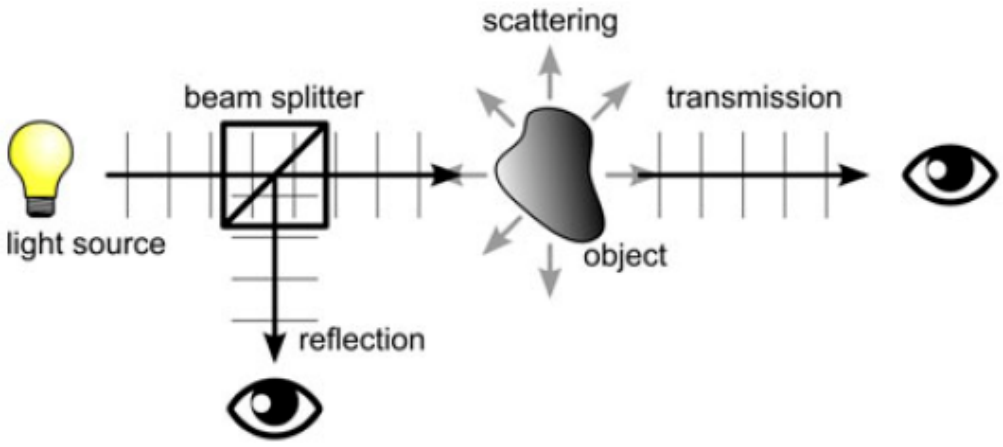

Figure 1.2: Sketch of a basic scheme for viewing an object in a microscope. The object is illuminated by a light source, and is observed either by reflection through its scattered light or in transmission by looking at the object's shadow, taken from Weisenburger et.al [12].

Looking at Figure 1.3 we see that the main geometries of microscopy are transmission and reflection. A light source illuminates with a certain power the sample which resides on a microscope glass slide. A portion of the incoming power is scattered by the sample, and another part will serve as reference power.

Once they reach the detector, the scattered and reference component will interfere with each other if their phase difference is less than the coherence length of the illumination beam (interference phenomena) .
However, another aspect to consider when applying measurements through the microscope is to understand the sensitivity of our instrumentation. In other words, what is the size of the smallest object that can be detected.
To have high sensitivity, a sufficiently large signal is needed from the object of desire, and the problem is that the signal usually decreases rapidly as the size of the object decreases. Therefore, it is necessary to collect the signal efficiently and use very sensitive detectors. The detector can be a point detector or a camera among many. The performance of a light detector can be generally described by its quantum efficiency, the available dynamic range and its time resolution[13].
The improvements implemented in microscopy are based on instrumentation and/or techniques that can guarantee: high resolution, high sensitivity and contrast. One widely used microscopic technique that succeeds in fulfilling these improvements is confocal microscopy[14].

1.2 Confocal Microscopy

As described in the previous section for wide field microscopy all the light is transmitted through the specimen. That means that the image will consist of both the light in focus on the focal plane of the lens and the light out of focus.
The confocal microscope essentially removes the out-of-focus light by inserting a pinhole at the image plane such that out-of-focus light does not reach the detector. Only light focused at the pinhole passes through it, all other light is scattered. The basic principle behind confocal microscopy is this use of spatial filtering to generate a focused spot of illumination[15]. The practical effect of this is that the image comes from a thin section of the sample,

and by scanning many thin sections through the sample, a very sharp three-dimensional image of the sample[16].

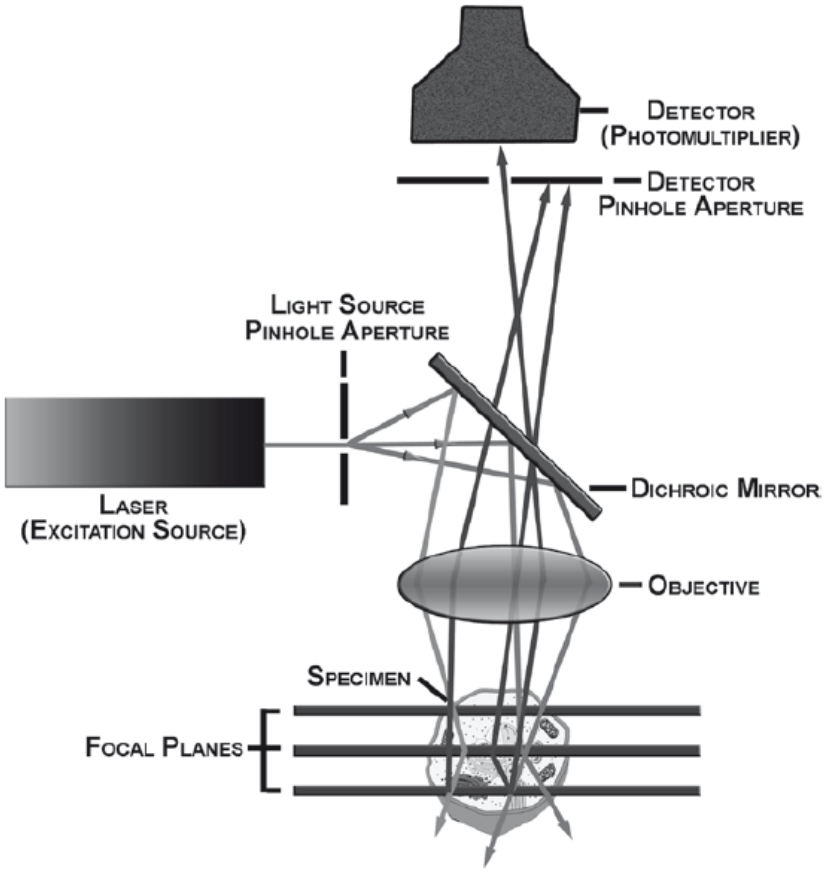

Figure 1.3: Schematic example of a Confocal Microscope taken from Leica[16].

A sensitive light detector, such as a photomultiplier tube, on the other side of the pinhole is used to detect the confocal light. This technique allows the specimen to be imaged one "point" at a time[14]. To create an image of the specimen, the focal spot is rapidly and serially scanned in the X-Y plane, which is why the confocal microscopes produce virtual horizontal cross-sectional images. As the scan proceeds, the signal from the detector

is sent to a computer that collects all the "point images" of the sample and builds the image in series, one pixel at a time. The sample is not actually cross-sectioned, but a sequence of virtual images are formed, which can be used for tomographic imaging. The images are displayed on a video monitor and the result is a sharp, high-contrast image , which could not be acquired with conventional light microscopy.

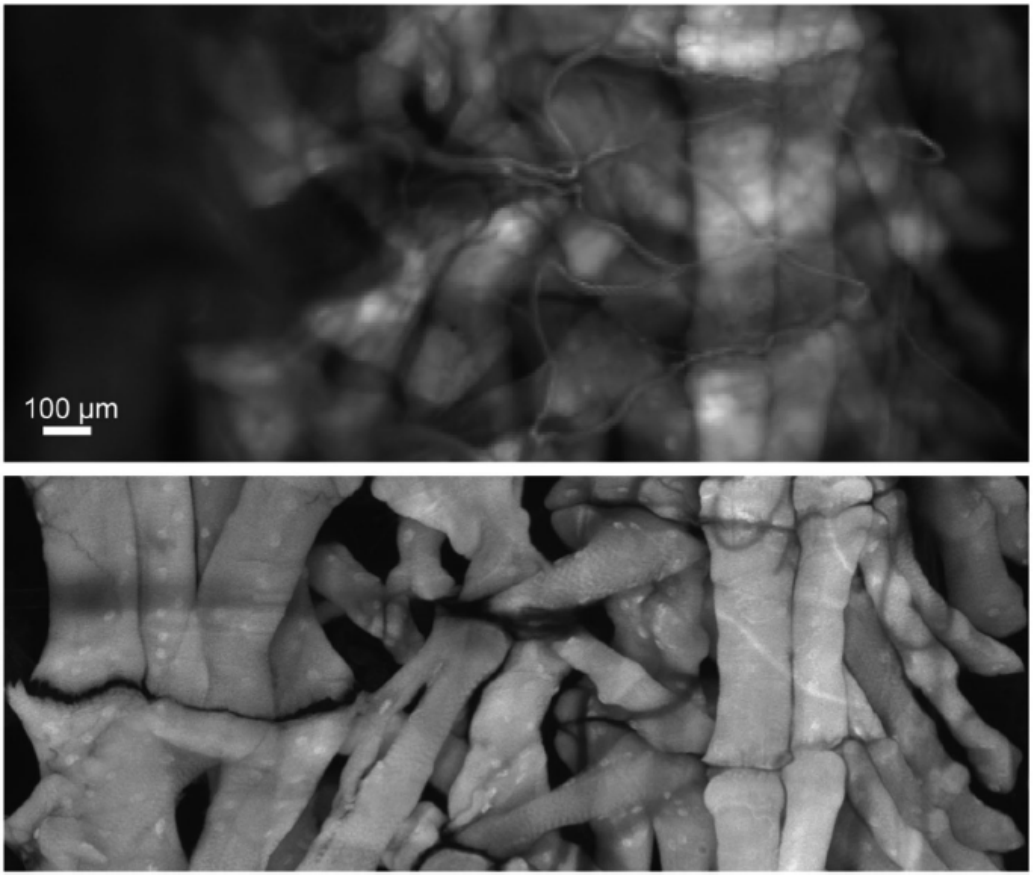

Figure 1.4: Widefield versus confocal microscopy. One hemisegment of a Drosophila larval fillet stained with AlexaFluor 647–conjugated phalloidin to label the musculature. The top picture is the widefield microscopy image and it can be seen that it is not as resolve as the bottom image that is the confocal's one. The confocal image took 2 h to build in a point scanning system, while the wide-field image was collected with an integration time of 1 s. Image taken from Elliot[17].

Image 1.4 provides a clear example of how the use of a pinhole allows to record only the light in focus and achieve images with higher resolution than classical microscopy (widefield). In fact, as explained in the previous section, it is very important to obtain well resolved and clear images to acquire information about the sample. Confocal microscopy allows this since

its resolution is:

$$d = \frac{0.8 \cdot \lambda}{2\text{NA}} \tag{1.5}$$

Since, as explained in the previous section, the resolution (according to the criterion of Rayleigh) in X and Y is determined by the distance from the center of Airy's disk to the first dark ring, for a confocal system, the pinhole radius is set slightly smaller than the radius of Airy's disk, and thus the X -Y resolution equation is what we get in Eq. 1.5

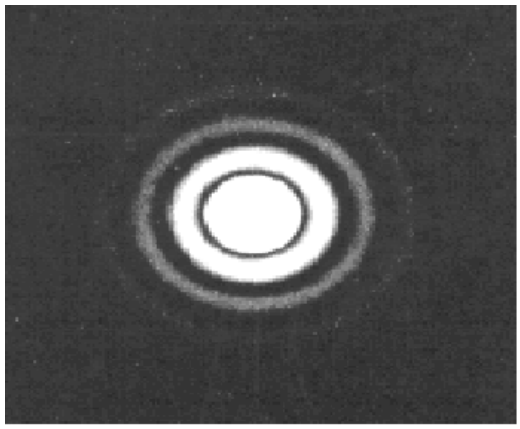

Figure 1.5: Example of Airy's disk[18].

The use of confocal microscopy may seem a gapless technique however there are issues when it comes to practical applications.
For example, the axial thickness of optical sections depends on the inverse of the square of NA. Therefore, when using low NA and low magnification objectives, the optical section may be 7 μm or more[15]. Cell walls, though, have smaller dimensions, so this technique is not convenient to use.
In addition, confocal imaging requires a balance between resolution, scan time, and sample photodestruction (Fig. 1.4). The higher the resolution, the longer the scan time and the longer the sample is exposed to the laser. Therefore, the probability of damaging the specimen increases.

1.3 Fluorescence Microscopy

Confocal microscopy can be performed in transmission or reflection mode for observing non fluorescent material. However, for most biological work, the confocal microscope is used in conjunction with fluorescent samples. Fluorescence imaging provides a specific, high contrast signal that maximally exploits the ability of the confocal microscope to remove out-of-focus light[19]. Fluorescence microscopy usually involves observing light in the visible range. although there are commercially available detectors such as charge coupled device (CCD) that detect both ultraviolet (UV) and infrared (IR) fluorescence.

The process behind fluorescence involves the absorption of energy (a photon) by an indicator (fluorophore), followed by the emission of some of this energy (as another photon with different wavelength) a few nanoseconds later[20]. The delay in emission is called fluorescence lifetime.

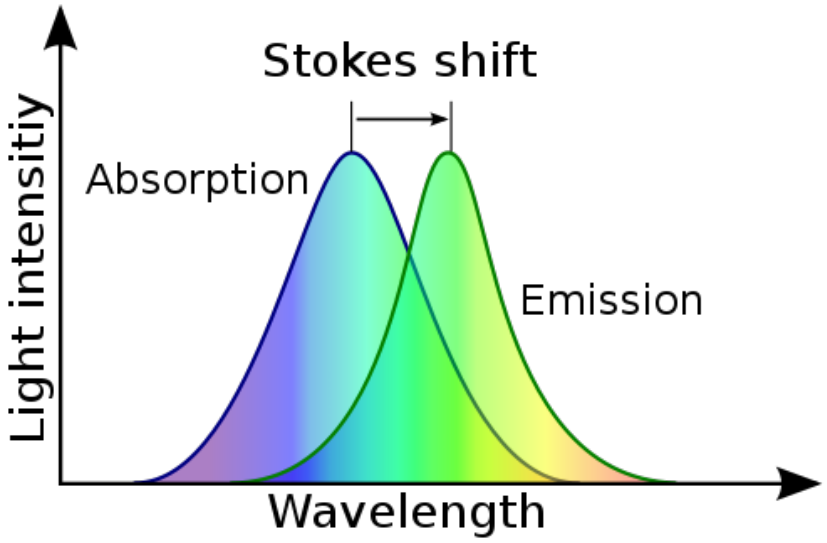

Figure 1.6: Diagram of the Stokes shift between absorption and emission light spectra. Picture taken from Wikipedia [21].

Before the process of emitting a photon, a very small part of the energy will be dissipated, so the emitted radiation will have lower energy than the absorbed radiation. The difference in energy between absorbed and emitted light is called Stoke's shift.

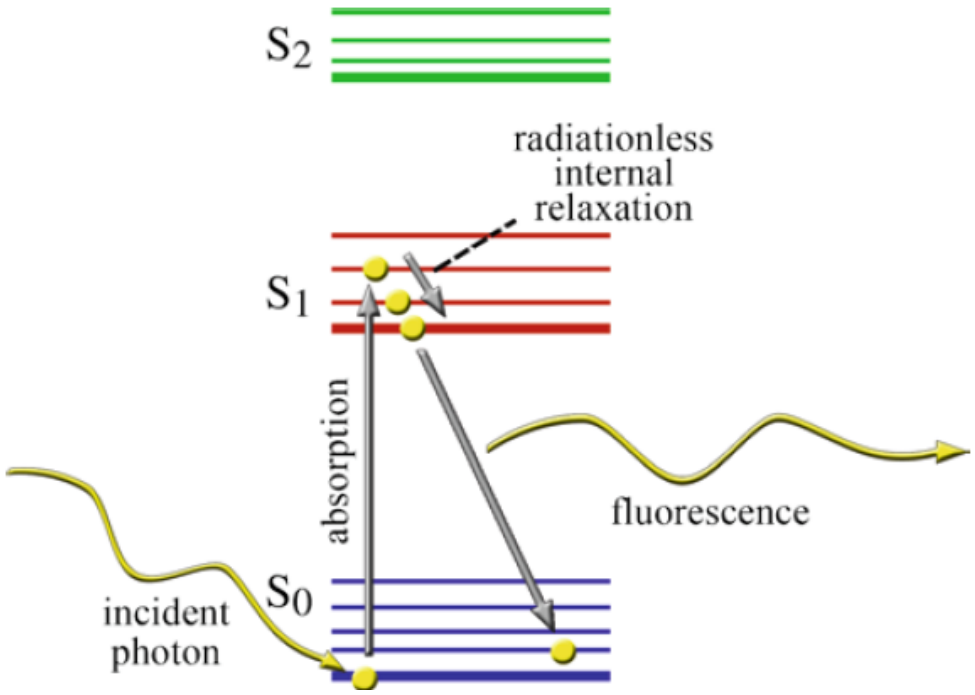

Figure 1.7: Example of excitation-emission cycle in fluorescence. When a fluorophore absorbs a photon it will be excited, so from its ground state, it will rise energetically to the first excited level. Thereafter there will be a relaxation and some of the energy will be released through heat. After this relaxation there is photon emission in the form of fluorescence and it will return to its ground level. Image taken from Gray et al[19].

The absorption and emission of photons by a fluorophore are best illustrated using a Jablonski energy diagram (Fig. 1.6). At room temperature the fluorophore will be in its lowest energy state (S_0). When absorption of light by the molecule occurs, it will absorb photon energy and through this will reach the excited state (S_1). Then there will be a relaxation of the flu-

orophore which will lead to a dissipation of energy, most often in the form of heat. Then the energy of the fluorochrome will be emitted as photons that will take it from the S_1 state to its original state. The energy emitted will be fluorescence. An additional important piece of information about a fluorophore is its quantum yield. This is the ratio of the number of photons emitted to the number of photons absorbed (Eq. 1.5) and is, therefore, a measure of the efficiency of fluorescence.

$$\Phi = \frac{\text{number of photons emitted}}{\text{number of photons absorbed}} \tag{1.6}$$

To harness the power of fluorescence it is necessary to make some modifications to the light optical microscope. It is necessary to provide a powerful light source that allows to reach specific different wavelengths for the fluorophores, a mechanism that illuminates only the fluorophore of interest and a means that allows to collect only the light coming from the fluorescence and not from other sources.
A suitable light source must be capable of providing a high flux of photons that will excite the fluorochrome of interest. High excitation levels are required because the fluorescence emission is usually low due to the fluorochrome. Furthermore, the fluorescent lamp must have a constant intensity throughout the irradiation time of the fluorophore. If it didn't have this feature, the final image would come out with uneven brightness.
The two commonly used lighting sources are mercury and xenon arc lamps as they are able to satisfy the criteria of uniformity and intensity. Both the lamps produce photons as a result of an arc flowing through an ionized gas. However, nowadays the use of LEDs or lasers as a light source is more and more frequent. Lasers produce an intense, monochromatic beam of light that is coherent and highly collimated.

In fluorescence microscopy, filters are often necessary for ensuring that only light emitted by a fluorochrome in the sample is passed on to the detector and for blocking any stray light in the system. In addition, filters

are needed to separate the various wavelengths of light emitted from different fluorochromes when using more than one color fluorochrome [19]. Due to a number of factors, the amount of light reaching the detector in a fluorescence microscope is relatively low. Even with very sensitive detectors, one still need to make sure that the signal strength is high enough against background noise. Otherwise, you cannot be sure of the accuracy of what is being detected. In order to maximize your signal, it is absolutely important to review the excitation and emission spectra of your fluorophores carefully and choose your filters based on these spectra.

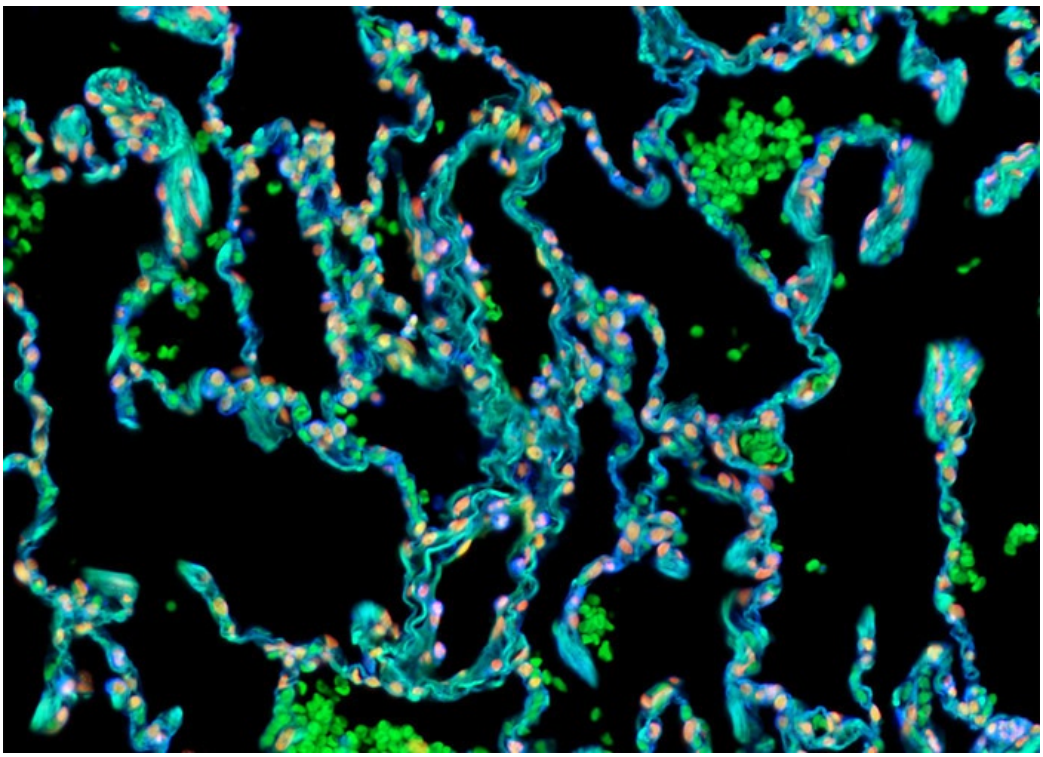

Figure 1.8: Example of Fluorescent image. The human lung tissue sample presented in the digital image above was labeled with Alexa Fluor 350 conjugated to the lectin wheat germ agglutinin. Image taken from Nikon[22].

1.4 Optical Coherence Tomography

Tomographic techniques generate cross section images of three-dimensional objects. Optical tomographic techniques are of particular importance in the medical field, because these techniques can provide non-invasive diagnostic images[2].

One of the most widely used techniques in ophthalmology is optical coherence tomography (OCT), a non-invasive method by which high axial resolution can be obtained[1]. It is a really prominent technique of the medical field because as can be seen in Figure 1.9 it has a higher resolution than other techniques.

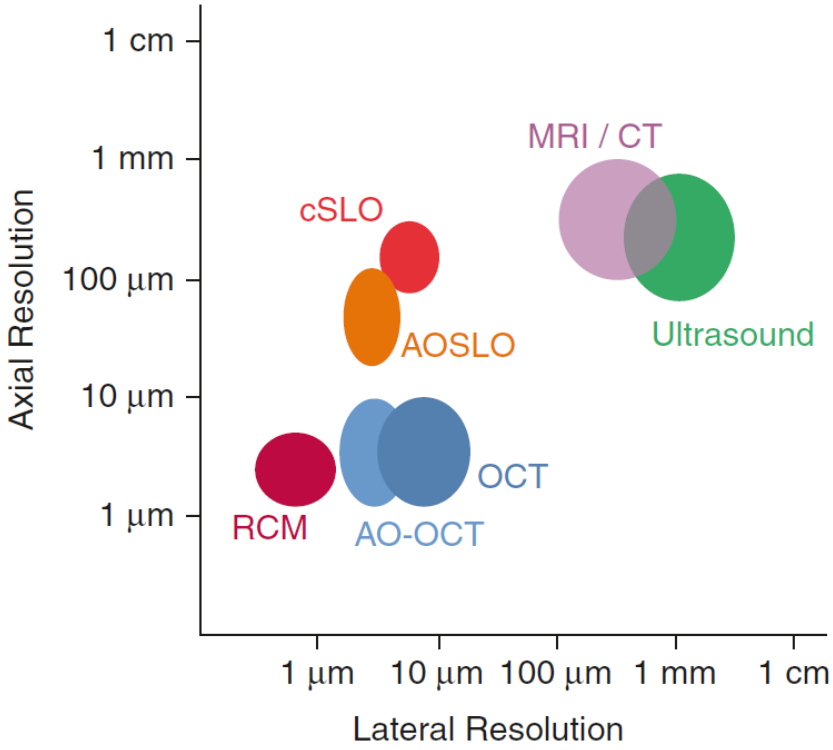

Figure 1.9: Comparison of resolution in axial and lateral direction between some medical imaging technique: reflectance confocal microscopy (RCM). confocal scanning laser ophthalmoscopy (cSLO), adaptive optics scanning laser ophthalmoscopy (AOSLO), optical coherence tomography (OCT), adaptive optics optical coherence tomography (AO-OCT).M agnetic resonance imaging (MRI), computed tomography (CT), medical ultrasound image taken from Aumann et al.[1].

The first OCT technique employes was derived from low-coherence interferometry [23]. Low-coherence interferometry measures the echo time delay and intensity of backscattered light by interfering it with light that has traveled a known reference path length and time delay[24]. Due to the interferometric measurement method, the axial resolution is defined by the light source and not by the focusing optics. The back-reflected waves are analyzed and their delay is measured to reveal the depth at which the reflection occurred. OCT uses light in the infrared range and an interferometer is used to

measure the delays of reflected waves that otherwise could not be measured. Through the use of this instrument, part of the light is directed at the sample and another part is sent to a reference arm and subsequently combines the two returning beams of light again. Under certain conditions, interference can be observed: coherent waves superimpose and their electromagnetic field amplitudes sum constructively (i.e., reinforce each other) or destructively (i.e., cancel each other out) or satisfy any condition in between.
The associated light intensity can be measured as an electrical signal using a photodetector which is the difference in the optical path length between the sample and the reference arm. Low coherence light sources (SLD) can be used however interference is only possible if the optical length paths are equal and have a low coherence length, usually on the order of micrometers[24].

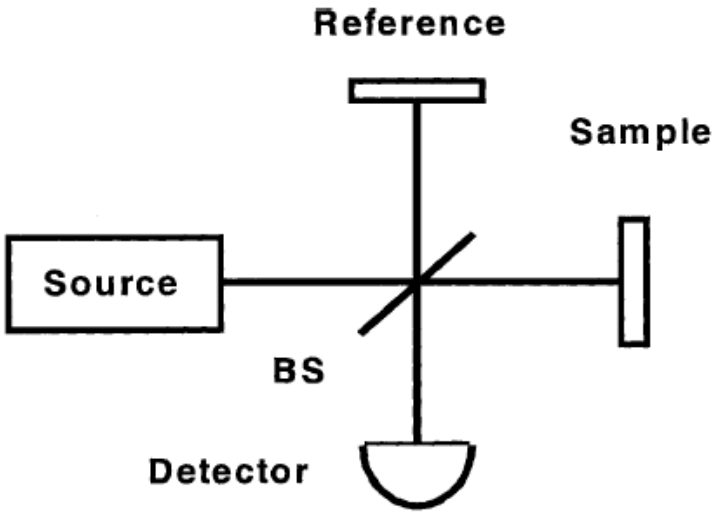

Figure 1.10: Schematic Representation of OCT. Light goes to the beam splitter (BS) and part of it goes to the sample and to the reference arm. The back scattered light goes back and its interference is detect by the detector. Image taken from Huang et al. [24].

1.4.1 OCT techinques

Many OCT-related techniques have been implemented in recent decades. One of the first techniques used was time domain OCT (TD-OCT).

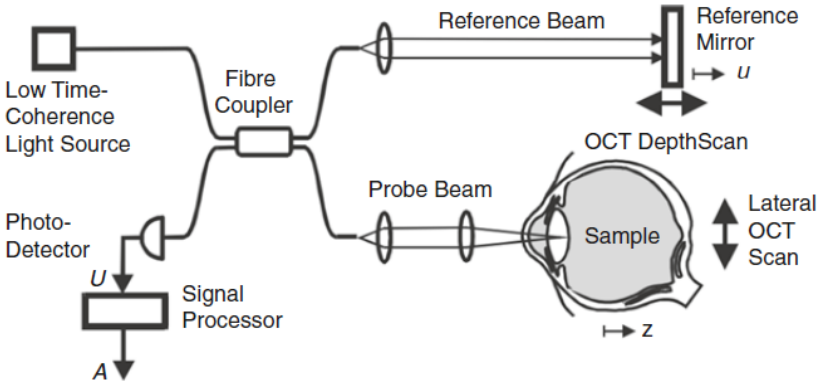

Figure 1.11: Schematic Set-up of TD-OCT. Image taken from Aumann et al. [1].

As depicted by Figure 1.11, the low-coherence light source is led to the interferometer in this case a fiber coupler (in other examples it may also be a beam splitter).The light is split, one part will reach the specimen the other will operate as a reference beam. The back-reflected light from both arms will combine and interfere if, as previously explained, the optical path length matches.

Modulations of intensity, also called "bursts" of interference fringe, are detected by the photodiode. The amount of reflection or back-scattering from the sample is obtained directly from the envelope of this signal[2] .

For each sample point, the reference mirror will perform a depth (z) scan, and each light intensity will be recorded by the photodetector. Implementing this scan produces a full depth profile of the sample reflectivity at the position of the beam, which is called an A-scan (amplitude scan)[23]. By collecting adjacent A-scans for successive pixels along a transversal coordinate, a cross-section image is obtained, termed as a B-scan[25].

OCT techniques have found over time many fields of application. However

TD-OCT is a very time-consuming technique, since one has to scan the whole sample. That is why a technique using a spectrometer was introduced like the Spectral domain OCT (SD-OCT) ,or also known as spectrometer based Fourier domain OCT. This technique records an interference spectrum, also known as an spectral interferogram, from which the A-scan is calculated by means of the Fourier transform.
The spectrometer uses a diffraction element to spatially separate the contributions of different wavelengths into a line image that is recorded by a high-speed line-scan camera. Each camera's read-out constitutes a spectral interferogram with an overlay of fringe patterns[1].
A superluminescent diode (SLD) is usually chosen as a light source because of its characteristic wide bandwidth and high output power.

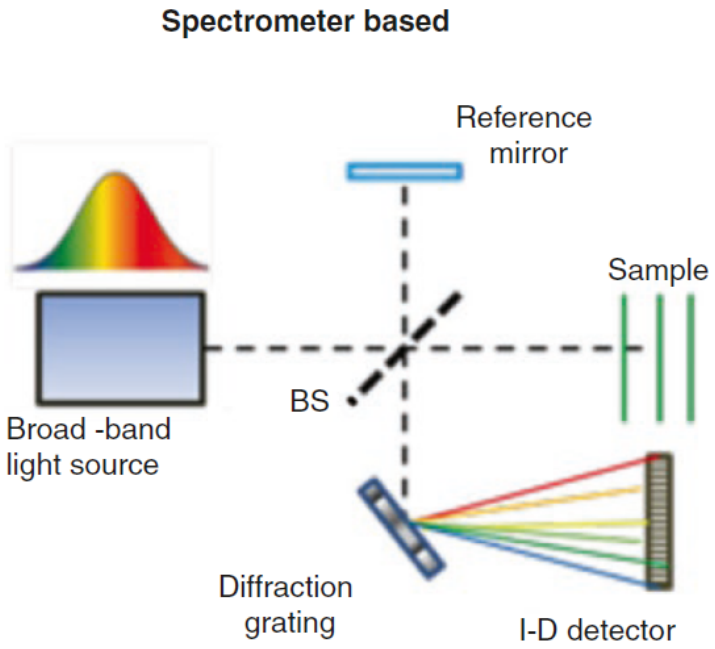

Figure 1.12: Schematic Set-up of SD-OCT. Image taken from Aumann et al. [1].

During a scanning, each wavelength component of the interferometric sig-

nal is sequentially detected by a high-speed photodetector. One wavelength constitutes a spectral interferogram with fringe patterns. For each sample point, the spectral interferogram is recorded as shown in Figure 1.13

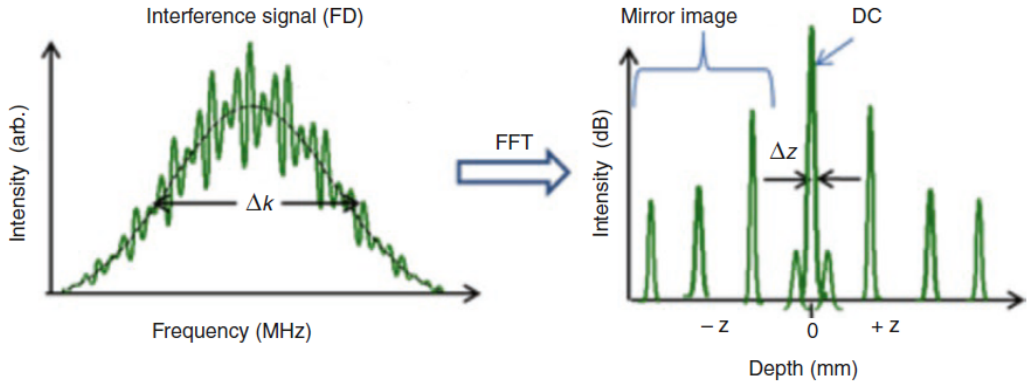

Figure 1.13: FFT is used to transform the interference signal into the A-scan.. Image taken from Drexel et al. [26].

In contrast to TD-OCT, the interferogram contains information for all depth layers of the sample simultaneously. The Fourier Transform is a necessary step to extract the individual contribution of their depth position. The amplitude of the complex-valued Fourier transform is squared to yield power values. As can be seen from Fig. 1.13 the A-scan contains a mirror image, which is related to the Fourier Transform itself and it will be not count in the final image.
Overall, compared to TD-OCT, the SD-OCT techniques have allowed for a dramatic increase in signal-to-noise ratio (SNR) and imaging speed[27, 28]. However the SD-OCT detector array are expensive and they have a small dinamic range[2].

Chapter 2

Materials and Methods

2.1 Experimental SetUp

In these experiments, a broadband light source, a superluminescent diode (SLD) (Superlum Inc., $\lambda_0 = 840$ nm, $\Delta\lambda = 160$ nm) is used to reduce the measurement's time, it eliminates the noise of the scanner and also minimizes other effects, such as fiber motion. Thanks to that an high axial resolution in the picometer range has been achieved.
The light is divided by a 2×2 fibre coupler and one output is coupled into an inverted microscope (Nikon E2000) where the sample is placed.
We focused the light on the samples with a microscope objective (Nikon 20x, NA = 0.75). The signal reflected from the sample is coupled back into the same fiber through a lens and part of it reaches a spectrometer (Wasatch Photonics, Cobra S-800) where the signal received is analysed by the computer (figure 2.1).
The spectrum is recorded by a line camera (E2V OCTAOLUS) with an 80 kHz line rate and a spectral resolution of 0.15 nm.
The 80/20 beam splitter inside the microscope side port allows for simultaneous sample visualization and interferometry.

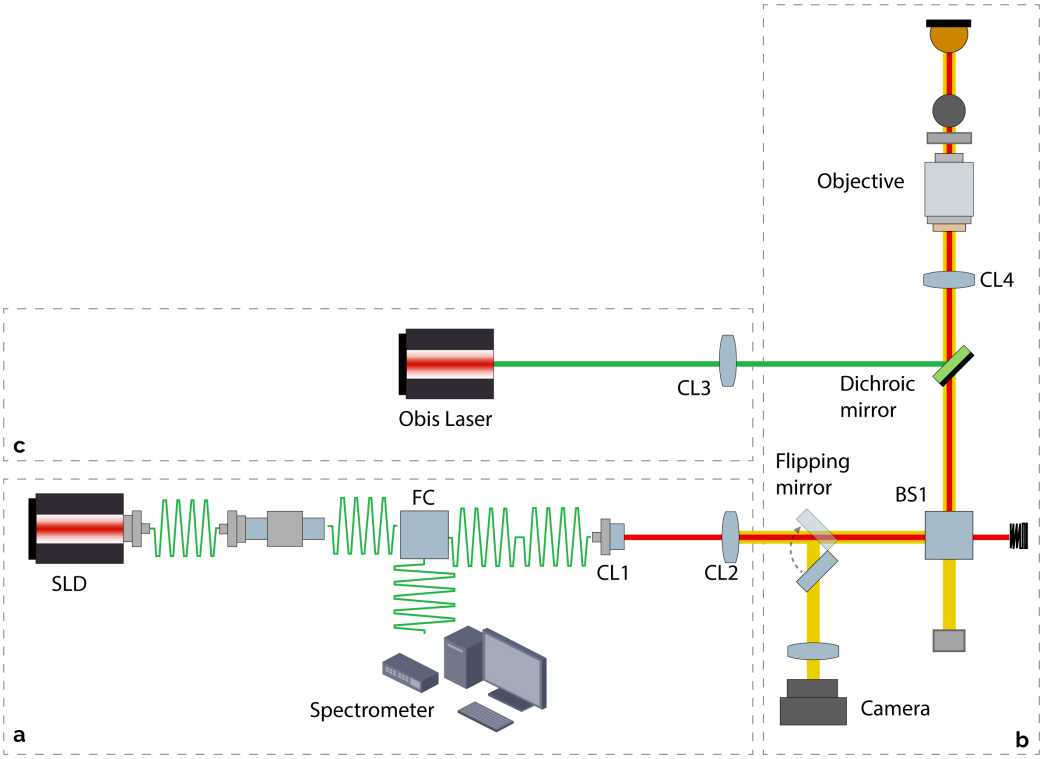

Figure 2.1: Setup of the SD-OCT system adapted from Asgari *et al.*[29].
(a) The light source and detection part includes a superluminescent light source (SLD), a fiber coupler (FC), a collimator (CL1), and spectrometer (SP). (b) Microscopy section where the light is directed to the sample by a collimated lens (CL2), BS1 (P), microscope objective, and arrives at the microsphere. (c) Excitation arm with a 532 nm laser, with a collimation lens (CL3).

The signal from the interference fringes of the sample is obtained with the following configuration. The reflection from the bottom surface of the sample trapped between the slides serves as the reference electric field, while the reflection from the top constitutes the sample field. In this configuration we detect the difference in the close-by reflection directly, that's why it was not required to use the reference arm.
To expand the beads by heat, an excitation arm to our set-up has been added. A fiber-coupled, 532 nm laser (Coherent Obis) has been connected to the ex-

citation port of the microscope, overlapping with the OCT beam using a Nikon G-2B cube (Long-pass Emission). This cube is usually equipped with a dichroic mirror, an excitation filter and a transmission filter. The dichroic mirror reflects the green light and allows the longer wavelengths to transmit. Since the transmission filter covers the same range of SD-OCT light source, it has been removed from the cube to avoid losing the SLD signal.
We modulated the laser with a function generator, controlled by a microcontroller (Arduino) with a modulation period of 88 ms and a duty cycle of 50%. The excitation light is collimated and focused, with the microscope objective, where the beam diameter is ≈ 4 μm and the Rayleigh length is larger than 10 μm.

2.2 Sample properties and preparation

In this thesis commercial polystyrene beads doped with fluorophores have been analyzed. The polystyrene microspheres provided by ThermoFisher FluoSpheres™ have a spherical shape with a diameter of 10 μm and present an orange fluorescence[30]. The concentration of the beads inside a flask was $C = 3,6 * 10^6$ beads/ml but the concentration of the fluorophores inside a single bead was not provided by the company.
The fluorophores presented an absorption peak at wavelength $\lambda_1 = 540$ nm and an emission peak at wavelength $\lambda_2 = 560$ nm this can be seen from the figure 2.2. For this reason, a laser in the highest absorption range in the microsphere spectrum was used, and the choice fell on the Coherent Obis laser with a wavelength of $\lambda = 532$ nm.

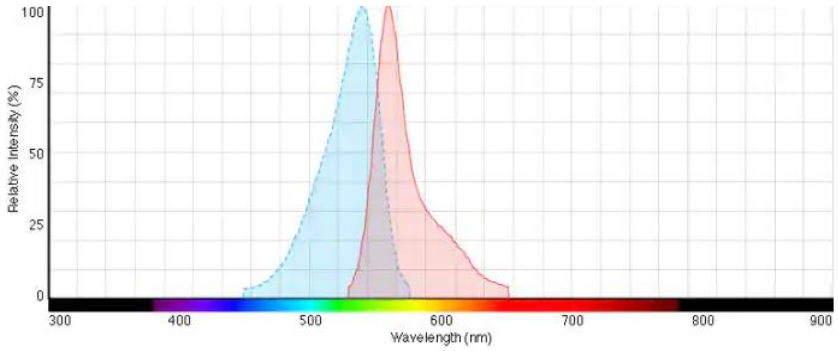

Figure 2.2: Fluorescence spectra of the sample provided by the company[30].

The sample chamber has been built by a coverslip (No. 1.5H; 22 x 22 mm), a spacer to make the chamber thickness = 100 μm and a microscope glass slide. A suspension of microspheres in agarose gel (1%) was deposited inside the chamber. The suspension of the beads in agarose was prepared by weighing.

0.1 gram of agarose was weighed on an analytical scale and then introduced into a beaker and dissolved in 10 ml of distilled water to obtain a 1% solution in volume. To prevent solidification, the solution was heated to 90°C under constant stirring.

After about fifteen minutes, 30 μl of the agarose solution was taken out and deposited in an Eppendorf tube and stored in a heater at 60°C.

In the meantime an imaging spacer was placed in the central part of the microscope glass slide so that when the sample is introduced, the coverslip can adhere and stick to it.

Next, 10 μl were taken from the solution containing the microspheres with fluorophores and introduced into the Eppendorf containing the agarose solution. After shaking the solution to allow the beads to spread, 10 μl of suspension of beads in agarose was deposited on the centre of the microscope glass slide. The cover-slip was placed carefully on top of it in order to cover the liquid completely.

The use of Agarose gel allows a certain distance between the surface of the coverslip and the beads to be maintained and prevents them from moving during the experiment.

2.3 Measurements

All the experiments were conducted using the instrumentation and sample described in the previous sections.
Python was used to actively control the data measurement. Through it, the necessary inputs for the measurement were entered. These inputs are required for measurement and data acquisition, the parameters inserted are in accordance with the purpose of the thesis and suitable for reliable and reproducible data. Of all the parameters, some are fixed others have been changed, the table below (Table 2.1) will give you an overview of the inputs and their meaning.

Inputs	**Meaning**	**Value**
ROI pixel1	Region of Interest starting pixel the spectrum starts in this pixel of the spectrometer	744
ROI pixel2	Region of Interest end pixel the spectrum ends in this pixel of the spectrometer	1944
line period	Line rapidity of the Octoplus camera in μs	value not fixed (20 or 50)
Exposure time	Exposure time value (in μs) cannot reach Line period value due to an integration dead time 0.7 μs	value not fixed (19.3 or 49.3)
Period cycle	Period cycle of the modulation laser in ms	100
Laser on	In each period of the heating laser cycle how long the laser was on in ms	88
Frames	How many frames are recorded	value not fixed (1600 or 4000)
Lines	How many lines are in each frame	50
Number of buffers	The buffer reserved for the camera to fill in a circle of recording	5
Trigger delay	How many frames the heating laser waits to start emitting	4
Number of cycles	Number of cycles of the heating laser	0
Power	Power of the green laser	Value not fixed (5 mW, 10 mW or 15 mW)
Refractive index	Refractive index of polystyrene	1.57
Diameter	Diameter of polystyrene microsphere in μm	10

Table 2.1: Measurements' inputs.

Measurements were carried out for three different laser powers: 5 mW, 10 mW and 15 mW. In addition to these, a measurement with zero laser power was performed.
However, the actual laser power reaching the sample differs from the initial one. It was recorded using an photodiode (UPD-300 SP) and the actual power for the three different measurements is: 3.12 mW, 7.4 mW and 10.8 mW; this is due to the energy loss of the laser beam during its path to the sample. Each measurement was run in duplicate for each laser power in order to ascertain the reproducibility of these analyses.

2.3.1 Expansion measurements

In one of these experiments the stabilty of the setup wanted to be investigated, so we decided to have 28 pulses of the laser. We set a high number of frames (the number of total frames is the product between frames and lines in the table 2.1, in this case 200000) in order to get lot of information for every pixel recorded. The exposure time and the line period were adjusted to perform the analysis in 4 seconds, the values were 19.3 μs and 20 μs respectively.

In addition some experiments where conducted to see the change in OPL only and not to verify the stability of the set-up. For the reason we decide to set a low number of frames (80000) and less pulses (14). In order to get the same time we configured the line period to 50 μs and the exposure time to 49.7 μs.

The experiments carried out with zero laser power was conducted in both ways just described.

2.3.2 Control measurements

These controlled experiments were conducted to investigate the influence of the axial movements on the baseline of the sample. The movements were

performed by turning the axial position control knob 50 nm each time. We have set the parameters as described in the previous subsection, however, to allow manual movement the line period has been assigned the value 100 in order to have a longer measurement. The same configuration was kept for measurements where there was ticking on the work table.

2.4 Analysis methods

In this thesis project, analyses were conducted using different software with similar properties, namely MatLab and Octave.
After experiments, the data obtained were saved with their parameters in the form of interferograms.
Through the application of mathematical functions, we were able to extract from them the informations required for the purpose of this thesis.
Below is a brief explanation of the functions involved in analysing the data (Figure 2.3).

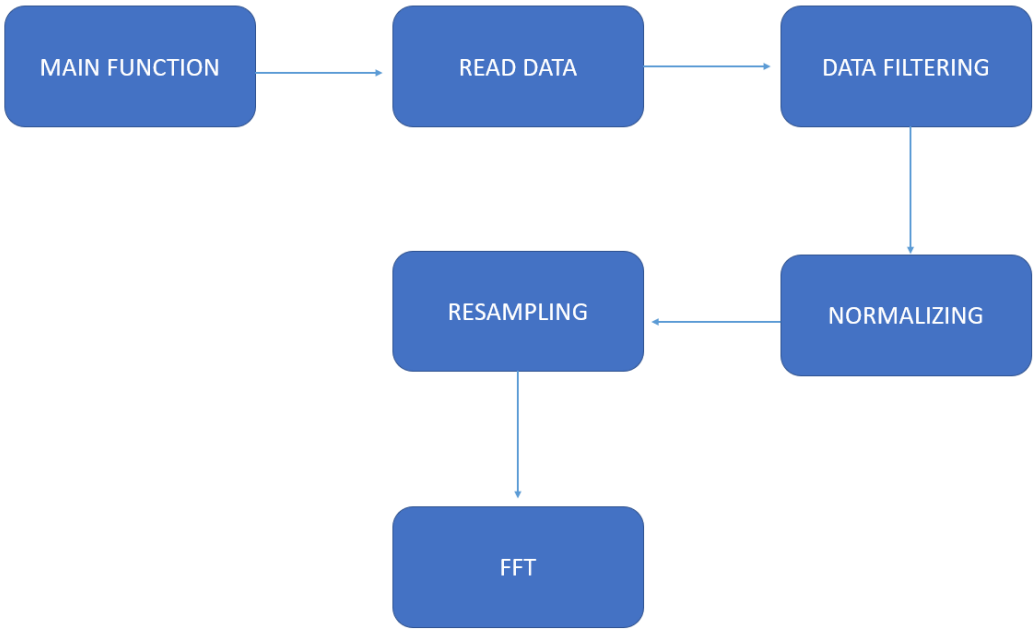

Figure 2.3: Schematic flow chart from interferogram to A-scan. The data recorded for each measurement are read and then mathematical functions(normalization and resampling) are applied to them, which will allow them to be read for the fourier transform from which we would obtain our results.

Having set up the main function from which all others are called, the first step was to read the data.
The read data are in the form of an interferogram consisting of 2048 pixels and a variable number of frames depending on the experiment (200000 or 80000).
Next, the data is filtered to obtain a homogeneous data set with corrections to adopt the Fourier Transform. Here among the different functions, the most important are normalisation and resampling.
For the analysis of the obtained data we will choose a part of the whole interferogram ranging from pixel 744 to 1944. The wavelengths included in these pixels range from 758 nm to 933 nm, as this is the interval of our SLD light source.

Then normalization of the data will be applied as we are not interested in the absolute value of intensity, so only the area underlying each intensity will be taken into account. Having dispersion in our data, we will apply via the spline function of MatLab a resampling of the data so that they have the same distance between pixels and thus are equally spaced in k-space. Once these corrections have been achieved, the Fourier Transform is applied in order to get the data from k space to z space.

Chapter 3

Theoretical Model

3.1 Heating model

In this project, a model that could fulfil all the assumptions we created has been built and then verified through the experimental part.
The development of a theoretical model provides a basis for better understanding and comprehension of how experiments and analyses work.
However, the actual factors affecting an experiment sometimes cannot be predicted theoretically because they are too random.
The experiments we conducted provided us with only indirect information. What we got from the data analysis was the optical path length without further information, but what we wanted to achieve was the actual expansion of the polystyrene beads. Thus, the creation of a theoretical model arises from the need to have direct information (actual size change) in relation to our thesis aim.

Our starting model is based on the expansion of microspheres. As previously described, the microspheres are doped with fluorophores, which, when hit by the laser beam, will absorb energy and subsequently emit fluorescence. Part of the energy will, however, be dissipated in the form of heat, which will cause the microsphere to expand. If we take into account that only the expansion of the microsphere occurs during heating, we will be able to calculate the variation of the optical path length of light,i.e. the thermal expansion.
The Optical path length (OPL), is the product of the geometric length of the path light follows through the system (z), and the index of refraction (n)

of the medium through which it propagates.[31]

$$OPL = 2n \cdot z \tag{3.1}$$

Where $n = 1.57$ for polystyrene and $z = 10$ μm, i.e. the diameter of the microsphere.

Optical path length is significant because it helps to determine the phase of light and control the interference and diffraction of light as it propagates.

A difference in optical path length between two paths is often called the optical path difference. The optical path difference between paths taken by two identical waves can be used to find phase change. Then using phase change, interference between the two waves can be calculated[31]. Given these statement, we would expect a positive and increasing OPL when the bead is hit by the laser beam.

However, when we collected the data, we noticed that the trend of the OPL was the opposite (i.e. negative) to our prediction. Not only expansion, but also another phenomenon during heating has to happen. One possibility is that a change in the refractive index also occurs during the process. Indeed there is a close correlation between refractive index and density[32]. When the polystyrene is subjected to heat the molecule will start to move more due to the temperature increase, this will lead to an extension of the bond length, which will cause the volume of the bead to expand. As the volume changes, the density also changes, and as a result, the refractive index will also be affected, since there is a close correlation between the refractive index and density (Fig. 3.1).

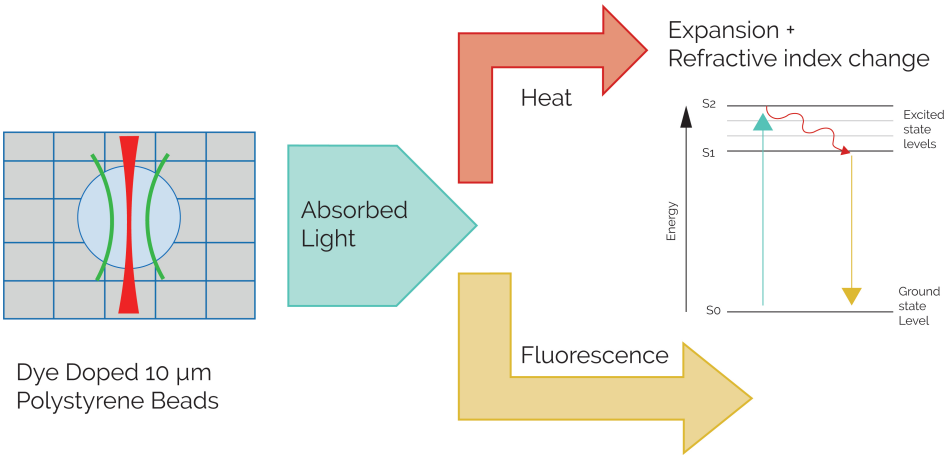

Figure 3.1: Schematic diagram of how the energy absorbed by a microsphere containing fluorophores is distributed. Part of the energy is released through heat which will cause expansion and a change in the refractive index of the bead, the other part will be emitted through fluorescence.

This deformation will lead to an increase in the size of the bead and thus also in the length of the light path. Through the light emitted by our broadband source (the SLD) we will be able to quantify the expansion of the microsphere by analysing the interference pattern between the light reflected at the bottom and the top of the bead surface.

Conducting a literature study that could support our theory, it was found that there is a close correlation between temperature rise and refractive index. In fact, as demonstrated by He at al.[33] when polystyrene is heated, the refractive index changes.

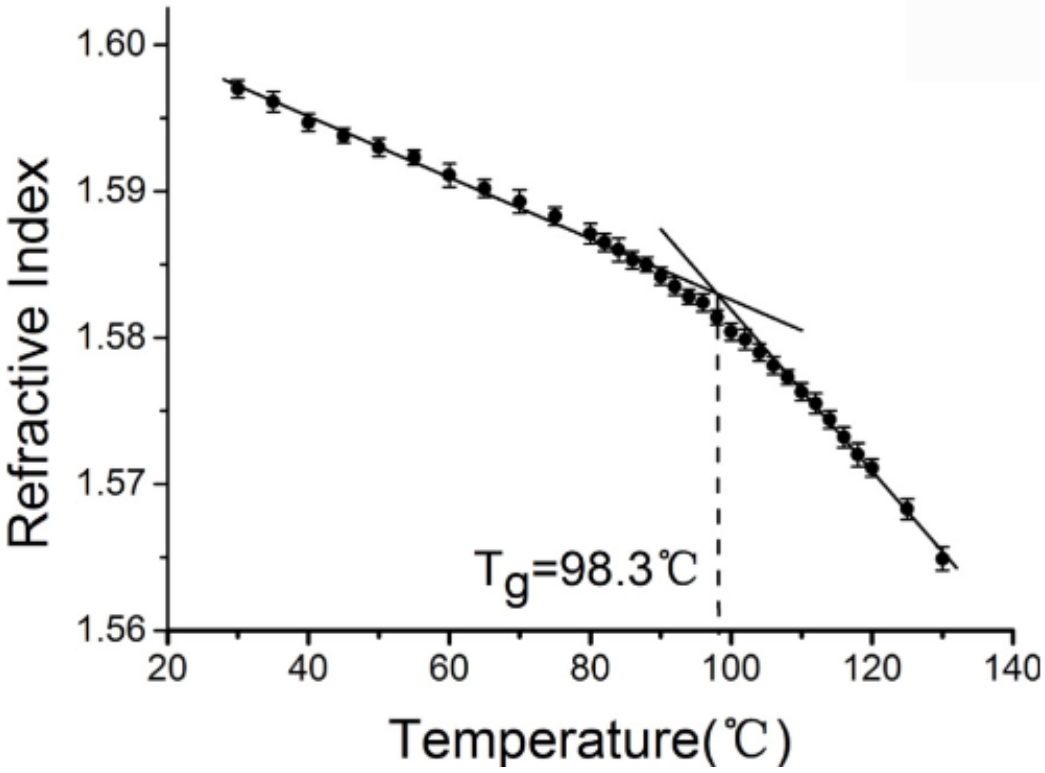

Figure 3.2: Figure 6(A) of He et al. [33] showing the temperature dependence of the optical index of a polystyrene bead.

From Figure 3.2 it can clearly be seen that as the temperature increases, the refractive index decreases. Subsequently we were able to calculate the slope of the line in relation to temperature and refractive index.
Taking the first four points of the curve shown in the Fig. 3.2, we tried to estimate the difference in refractive index in relation to temperature. We estimated that:

$$\frac{dn}{dT} = \frac{-0,01}{45K} = -2.2 \cdot 10^{-4}\mathrm{K}^{-1} \tag{3.2}$$

To support our estimation of $\frac{dn}{dT}$ based on He at al., we looked through the literature where we found a study on the dielectric constant as function

of temperature, this was conducted by Sasabe and Saito [34].

Polymer	T, °C	P, atm	$\left\langle \frac{d\varepsilon}{dT} \right\rangle$, K^{-1}	$\left\langle -\frac{(\varepsilon-1)(\varepsilon+2)}{3}\frac{d\ln V}{dT} \right\rangle$, K^{-1}	$\left\langle \frac{d\varepsilon}{dP} \right\rangle$, atm^{-1}	$\left\langle -\frac{(\varepsilon-1)(\varepsilon+1)}{3}\frac{d\ln V}{dP} \right\rangle$, atm^{-1}
PE-L	25—70	1	-0.54×10^{-3}	-0.50×10^{-3}		
	25	1—2000			4.39×10^{-5}	5.25×10^{-5}
	39	1—1000			4.35×10^{-5}	6.59×10^{-5}
PE-H	25—80	1	-0.89×10^{-3}	-1.19×10^{-3}		
	25	1—2000			3.75×10^{-5}	3.66×10^{-5}
	39	1—2000			4.10×10^{-5}	3.91×10^{-5}
PP	25—100	1	-1.12×10^{-3}	-0.66×10^{-3}		
	30	1—1000			4.3×10^{-5}	4.5×10^{-5}
	70	1—1000			3.5×10^{-5}	3.2×10^{-5}
PTFE	30—115	1	-0.78×10^{-3}	-0.68×10^{-3}		
	35	1—2000			3.78×10^{-5}	4.07×10^{-5}
	45	1—2000			3.52×10^{-5}	4.10×10^{-5}
PS	30—80	1	-0.66×10^{-3}	-0.82×10^{-3}		
	21	1—2000			5.55×10^{-5}	6.02×10^{-5}
	54	1—2000			5.14×10^{-5}	6.54×10^{-5}
	107	1—2000			8.00×10^{-5}	8.88×10^{-5}
	121	1—2000			9.46×10^{-5}	9.84×10^{-5}

Figure 3.3: Table 1 Sasabe and Saito [34]. Average contribution of variation in volume to temperature and pressure dependence of dielectric constant

Knowing the relation between refractive index n and dielectric constant ϵ equal to : $\epsilon = n^2$ [35], we are be able to estimate $\frac{dn}{dT}$:

$$\frac{dn}{dT} = \frac{1}{2} \cdot \frac{1}{n} \cdot \frac{\delta\epsilon}{\delta T} \tag{3.3}$$

n for polystyrene is equal to 1.57 and the value of $\frac{\delta\epsilon}{\delta T}$ is tabulated in figure 3.3. Having found this relation, we can calculate $\frac{dn}{dT}$ that is equal to:

$$\frac{dn}{dT} = -2.1 \cdot 10^{-4}\mathrm{K}^{-1} \tag{3.4}$$

The value just found is in a very good agreement with that calculated by He et al. so we can agree that the assumption regarding the change in refractive index as temperature changes finds a well-founded basis in the literature.

3.2 OPL derivation

Following the theoretical model explained in the previous section we will derive and calculate values based on the assumptions previously described. Having stated that like the diameter of the microsphere, the refractive index also changes with increasing temperature, the new formula for calculating OPL will be:

$$\text{OPL} = 2((n_0 + \Delta n)(z_0 + \Delta z) - n_0 z_0) \tag{3.5}$$

When we expand equation 3.5, by multiplying the two terms in brackets, we found the two $n_0 z_0$ terms have opposite signs and therefore will cancel. We assume at this step that the contribution of the term $\Delta n \Delta z$ is negligible compared to the others, because the expansion (Δz) will be in the range of nanometer and Δn will be in the range of 10^{-4} thus this factor can be neglected. The final equation will be:

$$\text{OPL} = 2((\Delta n z_0) + (n_0 \Delta z)) \tag{3.6}$$

This is the final equation to describe the change in OPL as a function of refractive index and size.
However we found $\Delta n = \frac{dn}{dT} \cdot \Delta T$ and furthermore, we can rewrite the change in dimension (Δz) using the linear expansion equation for which $\Delta z = \alpha z_0 \Delta T$, where α is the linear expansion coefficient of polystyrene. If we substitute in 3.7 we get:

$$\text{OPL} = 2(\frac{dn}{dT} \Delta T z_0) + (n_0 \alpha z_0 \Delta T) \tag{3.7}$$

Dividing the ΔOPL by ΔT we can find the relationship linking OPL to temperature as the other values in the equation are known.

$$\frac{\Delta OPL}{\Delta T} = 2(\frac{dn}{dT} z_0 + n_0 \alpha z_0) \tag{3.8}$$

The values entered and used to calculate the ratio are as follows:
$z_0 = 10\ \mu$m
$n_0 = 1.57$
$\frac{dn}{dT} = -2.2 \cdot 10^{-4}\mathrm{K}^{-1}$
$\alpha = 2.33 \cdot 10^{-5} K^{-1}$
Thus we obtain that the value of OPL in relation to temperature is:

$$\frac{\Delta OPL}{\Delta T} = -3.67 \text{ nm/K} \tag{3.9}$$

This relation will enable us to estimate the ΔT of the experiment for each data set, after experimental measurements of ΔOPL.
Having built the model which there is a close correlation between refractive index, size and temperature, we will now test how the parameters in the equation 3.8 affect it.

Parameter	Value	Change (0.10%)	Real change %	Influence
z_0 [nm]	10000	-0.01	0.10%	100.00%
n_0	1.57	0.00	-0.02%	-19.98%
dn/dT [K^{-1}]	-2.20*10^{-4}	-0.0088	0.12%	119.98%
α [K^{-1}]	2.33*10^{-5}	0.00	-0.02%	-19.98%

Table 3.1: Influence of the parameters in the equation 3.8 by changing them of 0.10%.

As it can be seen from table 3.1 the term z_0 is the second most important and the scaling parameter in the equation 3.8 . It is the greatest value in the formula and by only changing it over 0.1% it will affect the equation by a factor of 100%.
The term dn/dT also affects a lot the equation by more than 100%, as we based our model on the refractive index change, we expected a great influence of this parameter. The parameters n_0 and α slightly change in the equation,

both of them influence my equation of about 20%.

Chapter 4

Results and Discussion

In this section, the data collected during the experiments will be presented, analysed and discussed. For each data set, the OPL difference, the position of the reflection peak (i.e. where the reflection occurs) and its magnitude will be described.
All these parameters were determined by investigating the upper part of the peak at the A-scan.

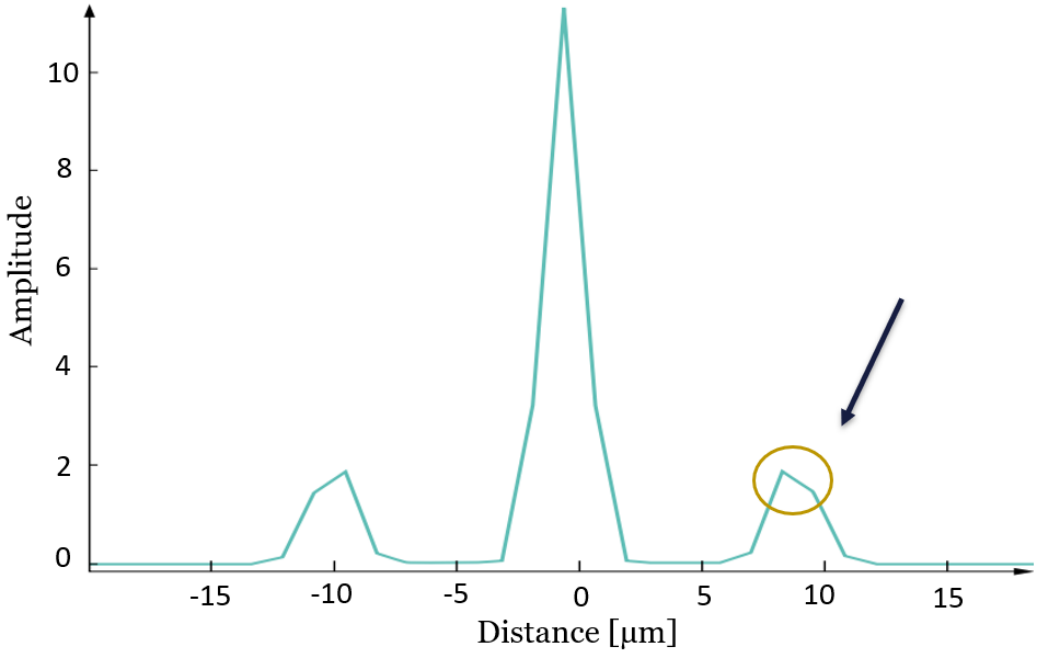

Figure 4.1: Example of A-Scan of the beads. Through the use of Fourier Transform we were able to extract the individual contribution of the depth position of the reflection. The circled area represents the region of interest of our analysis.

The arrow and the circled area in Figure 4.1 denote the region of the peak where the data were acquired and where the reflection phenomenon occurred. Since the A-scan is given by the Fourier Transform we will find 2 peaks, as the negative side is the mirror image built by the Fourier Transform itself, by convention we will consider only the positive peak.

4.1 Control measurements

The experiments conducted without laser irradiation on the microspheres allowed us to set the baseline of the sample and identify the sensitivity of the setup. Since there is no external source of irradiation, what we expect a continuous path with no fluctuations.

Graphs 4.2 represent our results for the measurements without heating by the laser. We have plotted in the y-axis the difference in the optical path length, the amplitude of the peak and its position against the time taken for the analysis (x-axis).
The difference in the optical path length of the light indicates how much the expansion occured during the measurements' time and it is based on the difference in reflection between the top and bottom of the beads surface. However, in this control experiment the laser power was set at 0 mW so no expansion occurred, but from this measurement we could see the stability (baseline) and sensitivity (noise) of the system. The peak position is a fitting result of the peak from the FFT in figure 4.1 using Jains' method and it is the structure at the certain size in the beam. Amplitude here is the maximum value of the peak in the Fourier Transform which we take as measure of the amplitude of the fringe. Both peak position and amplitude have been plotted against the time to see the variation of them during the measurements. All experiments carried out, reported that the set up we used is very sensitive to changes in OPL. As can be seen from the figure 4.2, we were able to achieve a sensitivity in the picometre range. Furthermore, the baseline, i.e the line at

the minimum value, is very stable throughout the experiment, we can esteem shifts of the order of 0.2 nm.
To prove the stability of the data obtained, observing the position of the peak during the analysis and its magnitude, can also be seen to be equally stable.

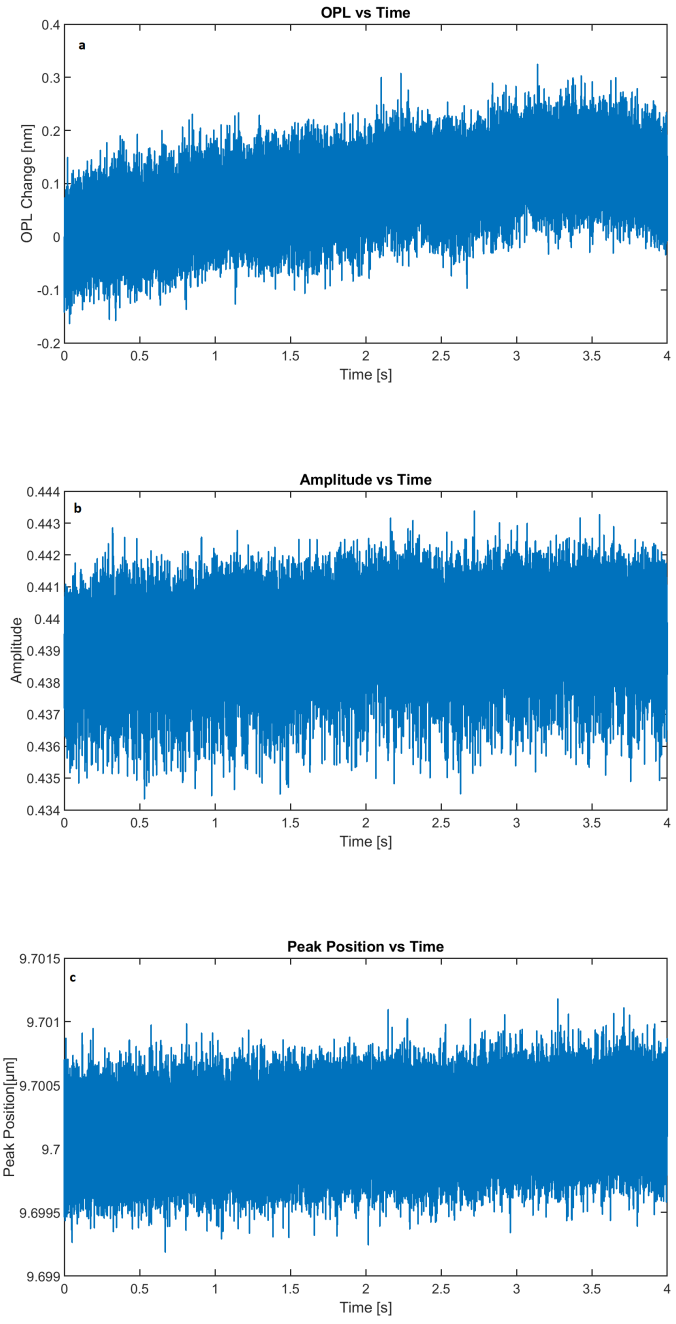

Figure 4.2: 0 mW measurements. (a) OPL change. (b) Amplitude of the peak. (c) Peak position

The position of the peak and its intensity are further verification of the reliability of the technique and the set-up used, in fact the fluctuation of the latter is very slight and constant during the measurements.
However, having a sensitivity in the picometre range, the instrumentation will be very sensitive to external factors affecting the performance of the measurement. To evaluate the stability of the collected data, we first calculated the Fourier transform of the phase and then the square of it.
Then using Parseval's theorem, analysing the area at high frequencies, we were able to obtain an estimation of the background noise without taking into account any artefacts or features.
To test how sensitive our set-up is, I tapped on the work table. The data collected (Fig. 4.3) show that even the slightest tapping can bring variation to the experiment. For both the phase, amplitude and position of the peak we can see that with each hit there is a substantial and clearly visible increase. We can conclude that even the slightest external factor can affect the measurements.

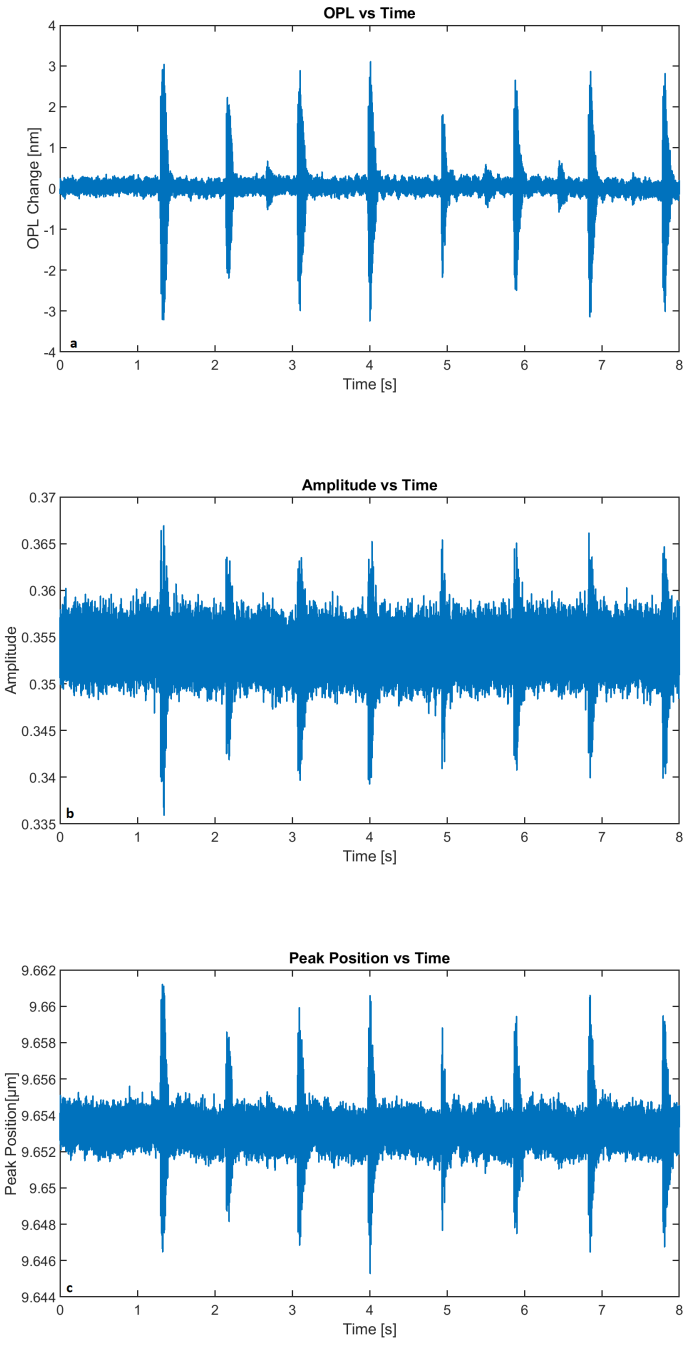

Figure 4.3: Tapping measurments with no laser power. (a) Phase of the sample. (b) Magnitude of the peak. (c) Peak position

4.2 Expansion measurements

The use of lasers in the experiments allowed us to expand the microspheres by heat. Here, the change in OPL was subsequently calculated and analysed between the different laser powers: 5 mW, 10 mW, 15 mW and look for similar behaviour for the different microspheres. What we expect to see from these experiments is a substantial increase in the size of the microsphere as the laser power is increased. Since there is a modulation of the laser, it is switched on and off in 88 ms intervals, we would expect to see two distinct jumps: one due to the heating of the laser and one due to the cooling of the microsphere when the laser is switched off. As the laser modulation has a rectangular profile we foresee that the jumps will maintain the same profile for the whole modulation's time. From the difference of the two jumps we can extrapolate the difference of the optical path length of light, i.e. the expansion. In addition the baseline should return to its starting point, i.e. to zero before the heating occured. However we did not see a perfect rectangular signal but a shape with exponential behaviour when temperature changes. In order to understand and quantify the thermal expansion, for each measurements, a fit of the profile of the pulse on and off has been coded. The function used for the fit was set as exponential in the form of:

$$k_s t + A \sum_i \alpha_i e^{-k_i t} \tag{4.1}$$

where the k_s is the linear correction factor in relation to the time t, A and α refer to the amplitude respectively the height and how strong is the component to reach the amplitude and $k_i t$ is the exponential rate. This function allows to calculate the signal at the start value of the laser when it is switched on and off. Furthermore, by calculating the difference of the peaks when the pulses are turned on and off, it is possible to determine the ΔOPL for each measurements.

For the sample collected we calculated the average OPL and the standard deviation. Then by applying the two (σ) sigma criteria, we were able to delineate which of our results were to be excluded in accordance with the criteria. Two standard deviations or two sigma, plotted above or below the mean value on the normal distribution curve, would define a region comprising 95% of all data points. We only excluded the values of OPL that where outside that region[36]. Subsequently, we wanted to test whether there is a difference in using 14 or 28 pluses of the laser. To verify this we used the t-test. A t-test is any statistical hypothesis test in which the test statistic follows a Student's t-distribution under the null hypothesis[37].
Like other tests, there are two kinds of hypotheses; null hypothesis and alternative hypothesis. The alternative hypothesis assumes that there is a statistically significant difference exists between the means, whereas the null hypothesis assumes that there is no statistically significant difference exists between the means[38].
We performed the calculation using a function inside Microsoft Excel.During the test, Excel calculates and displays the difference probability percentages. A t-test function can calculate one-tailed and two-tailed distribution methods. One-tailed tests gauge data relationships in one direction, while two-tailed tests check them for both directions. For example, a one-tailed test helps when one data set influences another, two-tailed tests may check data sets that influence each other, to know if our values are null or not we should compare t stat and t critical (two tail).
When t stat being smaller than t critical (two-tail), we can conclude that there is no statistically significant difference between the means[39].

Having defined the preliminary steps for understanding the data now they will be shown. In sequence they will be shown first for all three all graphs concerning the OPLs for the three laser powers and then the peak position and amplitude, respectively. Also the average OPL and t-test for each laser power will be displayed.

The figure below are plotted the OPL versus the time. As previously described the downward jump is the moment when the laser is on, the upward one is the cooling of the beads, i.e. when the laser is off, and when the modulation stops the baseline should return to its initial value. What can be seen from the figure is that all of them show the difference in the moment where the pulse are on and off. As the laser power increases, this difference also increases, leading to greater expansion of the microsphere. However it can be seen for 10 mW and 15 mW sample that the baseline does not came back to the initial value, this could be related to different factors, more explanations will be given in the next sections.

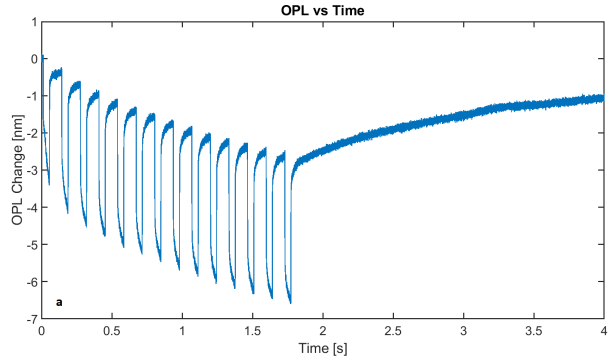

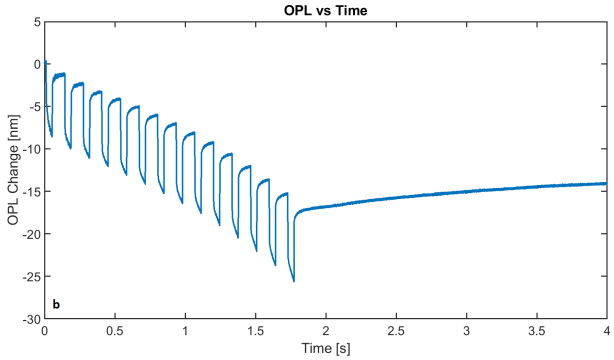

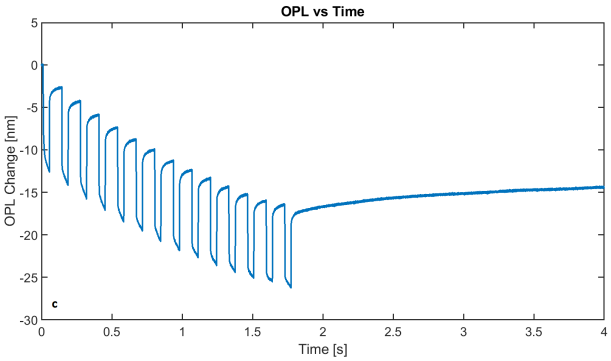

Figure 4.4: Example of OPL change with 14 pulses for the three different laser power. (a) 5 mW, (b) 10 mW, (c) 15 mW. The three figures show that as laser power increases, expansion also grows.

Then the fit function was applied to all measured samples to be able to calculate the average expansion for all laser powers. For the data recorded in the tables below, the standard deviation was calculated and 2 sigma criterion was implemented so that those not in agreement with the criterion could be identified. It was possible to recognize that for the data collected for 5 mw laser power all are in agreement with the criteria while for the other two powers the data marked with red color were discarded as not within the limit values of the criterion.

It must be mentioned that all OPL values were considered in their absolute values, since as explained in the previous chapter we have noted a negative trend.

Sample	ΔOPL 5 mW [nm]	n° of pulses
1	3.18	28
2	3.45	28
3	3.34	14
4	3.61	14
5	3.34	14
6	3.72	14
7	1.85	14
8	2.21	14
9	3.4	14
10	1.85	28
11	1.92	28
12	2.39	28
13	1.33	28
14	1.62	28
15	2.68	28
16	3.2	28
17	3.81	28
18	4.36	28

Sample	ΔOPL 10 mW [nm]	n° of pulses
1	7.51	14
2	7.89	14
3	7.95	14
4	8.3	14
5	5.02	14
6	5.74	14
7	7.68	14
8	5.45	28
9	5.61	28
10	7.02	28
11	11.21	28
12	3.85	28
13	5	28
14	7.36	28
15	8.34	28
16	8.39	28
17	8.09	28

Sample	ΔOPL 15 mW [nm]	n° of pulses
1	12.21	14
2	11.23	14
3	12.68	14
4	9.27	14
5	11.75	14
6	16.12	14
7	15.52	14
8	16.12	14
9	12.46	14
10	14.79	28
11	14.03	28
12	16.26	28
13	29.74	28
14	14.44	28
15	20.73	28
16	11.68	28
17	10.05	28
18	8.11	28

Table 4.1: Three diffrent table for the sample measured. The table on the left shows the ΔOPL for 5 mW, the table on the right shows the ΔOPL for 10 mW and the bottom table shows the ΔOPL for 15 mW.

Having calculated the averages for the various experiments (along with their standard deviations) it was then possible to calculate the difference

temperature value for the different powers by exploiting the relationship 3.9 and taking the value found in its absolute value.

	5 mW	**10 mW**	**15 mW**
OPL	2.85 ± 0.86 nm	7.02 ± 1.24 nm	12.92 ± 2.46 nm
ΔT	0.78 ± 0.23 K	1.91 ± 0.33 K	3.52 ± 0.67 K

Table 4.2: Values of the average of OPL (OPL) for the three different laser power and the difference in temperature (ΔT) calculated by the eq. 3.9.

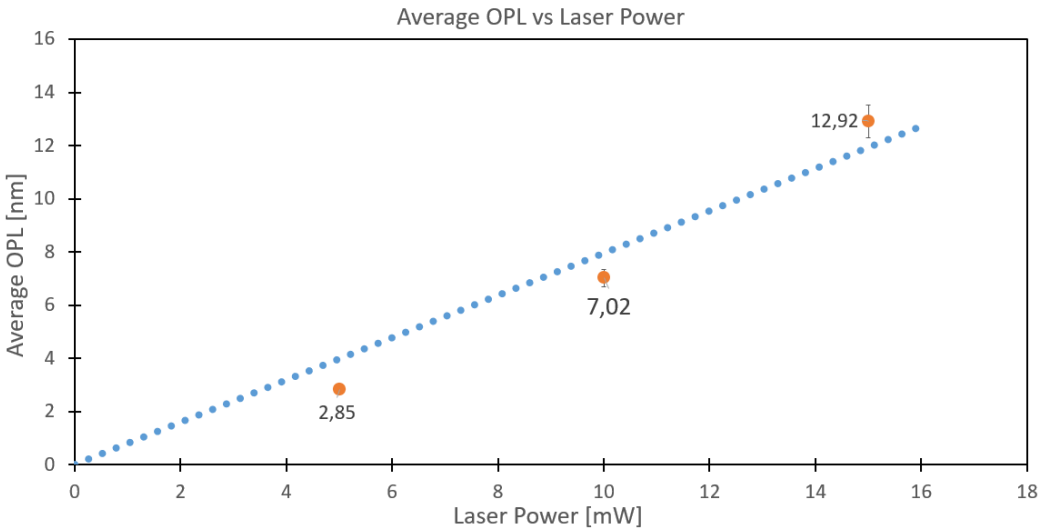

Figure 4.5: Average OPL vs Laser power. In this graph the dot line represents linear trend line.

The relationship that can be seen between the different expansions in relation to the laser powers is shown in Figure 4.7. It can be observed that the linear trend line (dot line) does not cross the experimental data obtained. The relationship is not perfectly linear as the value for the 15 mW appears to deviate but we have too little data (not enough different powers) to be sure. After conducting the analysis on the expansion, the position of the peak and its amplitude were also examined.

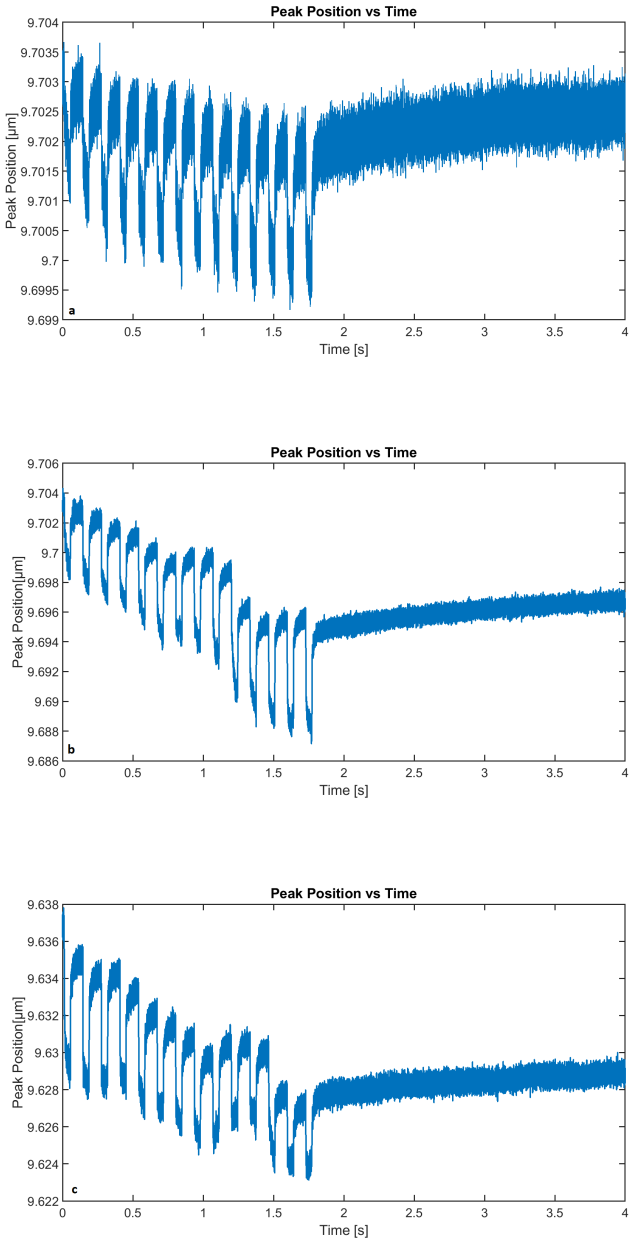

Figure 4.6: Peak position of the OPL measurements, previously shown, for the three different laser power. (a) 5 mW, (b) 10 mW, (c) 15 mW.

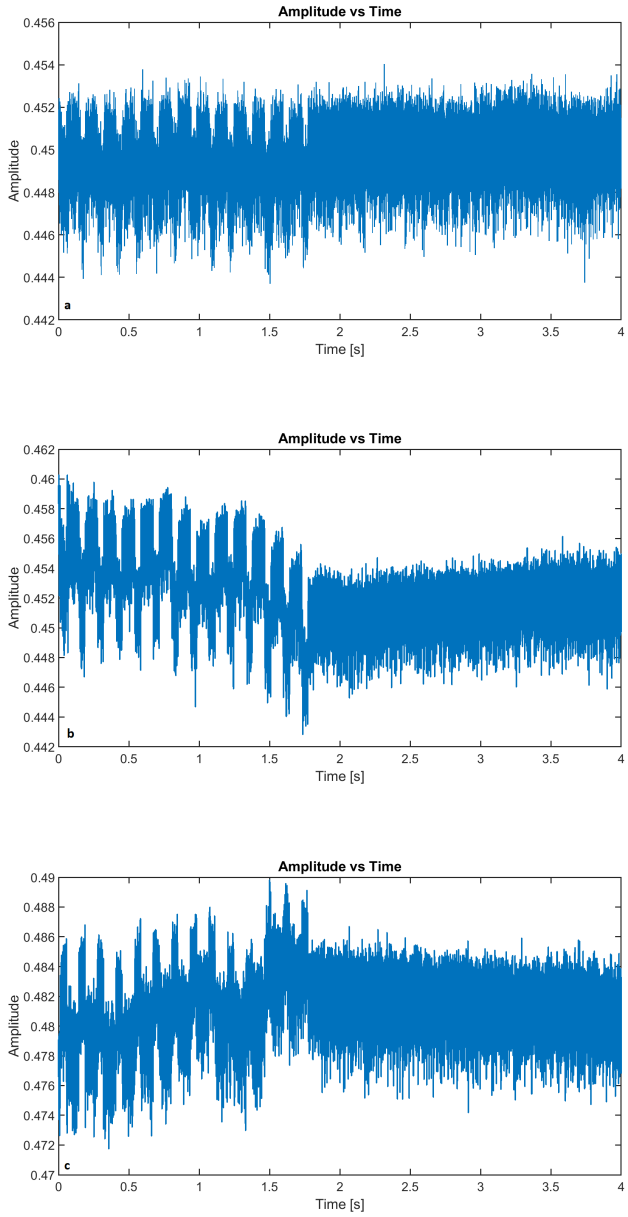

Figure 4.7: Amplitude of the peak for the three different laser power. (a) 5 mW, (b) 10 mW, (c) 15 mW.

For all the expansion experiments conducted, it can be noted that the laser also influenced the trend of both the peak position and its amplitude.

As might have been expected, as laser power increases, this leads to visible changes in graph outlines. If for the analyses carried out with 5 mW and 10 mW we recorded a negative but steady trend, for 15mW we noticed that among the results it is difficult to find a well-defined trend in fact many samples show different behaviors. To test whether this different trend is given by the different number of pulses, we compared the different data for each power between the different pulses: 14 or 28. By running the T-test through Excel (explained above) we could see that for all laser powers there is no substantial difference between the 2 average values. This was possible to identify because as shown in the tables below(4.3,4.4,4.5) all T stat values are less than T Critical (two tail) and this means that all values are within the confidence interval and therefore it can be agreed that the number of pulses does not significantly affect the measurements.

	14 pulses	*28 pulses*
Mean	3.067	2.708
Variance	0.533	0.950
Observations	7	11
Hypothesized Mean Difference	0	
df	15	
t Stat	0.891	
P(T<=t) one-tail	0.194	
t Critical one-tail	1.753	
P(T<=t) two-tail	0.387	
t Critical two-tail	2.131	

Table 4.3: t-test analysis carried out for 5 mW samples

	14 pulses	*28 pulses*
Mean	7.156	6.908
Variance	1.574	1.902
Observations	7	8
Hypothesized Mean Difference	0	
df	13	
t Stat	0.365	
P(T<=t) one-tail	0.361	
t Critical one-tail	1.771	
P(T<=t) two-tail	0.721	
t Critical two-tail	2.160	

Table 4.4: t-test analysis carried out for 10 mW samples

	14 pulses	*28 pulses*
Mean	13.04	12.766
Variance	5.678	8.489
Observations	9	7
Hypothesized Mean Difference	0	
df	12	
t Stat	0.202	
P(T<=t) one-tail	0.422	
t Critical one-tail	1.782	
P(T<=t) two-tail	0.843	
t Critical two-tail	2.179	

Table 4.5: t-test analysis carried out for 15 mW samples

In the Next section a further explanation of the data obtained will be given in relation to the theoretical model we created.

4.3 Discussion

In this section our theoretical model will be discussed in relation to the results obtained. Inconsistencies and points where our model works will be analyzed.

4.3.1 Discarded dataset

From the OPL calculations previously performed, we could see that some data were discarded because they did not fit within the limits of the criteria (2σ) we adopted. Looking at the data, we could see that other phenomena, unknown to us, influenced the measurements. We will also try to give a plausible explanation for the inconsistencies in our theoretical model.

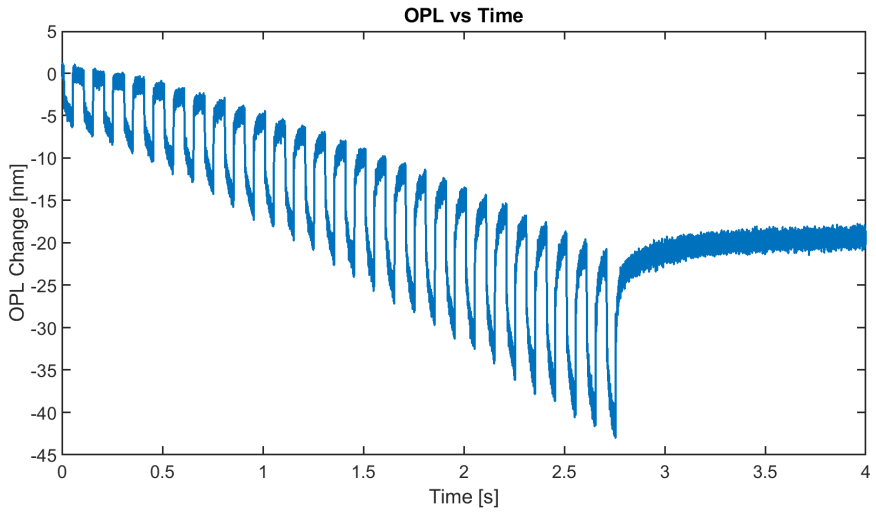

Figure 4.8: OPL of a discarded dataset of 10 mW

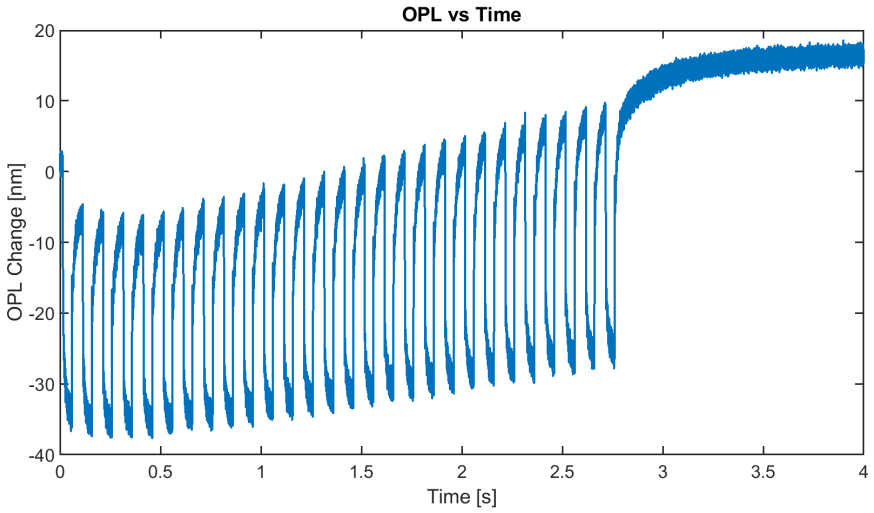

Figure 4.9: OPL of a discarded dataset of 15 mW

As can be seen from Figures 4.8 and 4.9, both display anomalous behavior. In the 10 mW case we can see how the amplitude goes up with temperature. This trend, Figure 4.8, is atypical because amplitude keeps rising as if it never reaches an equilibrium.

Figure 4.9 displays a positive trend different from the one we discussed in the previous sections. Looking at the fringe visibility as well (Fig 4.10 an 4.11), we will notice how the trend is incongruent with our assumptions. Furthermore, we can see how the amplitude is significantly lower than the data explained in the previous section where they displayed a value about 0.45.

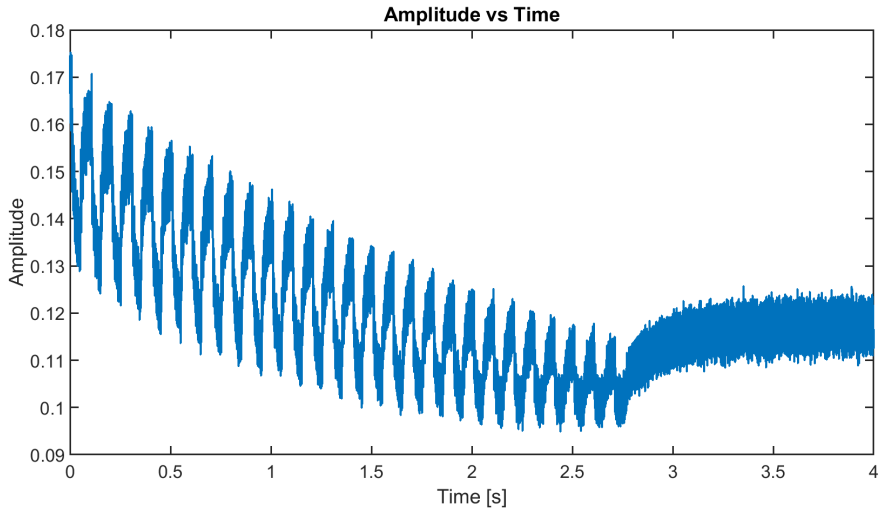

Figure 4.10: Magnitude of a discarded dataset of 10 mW

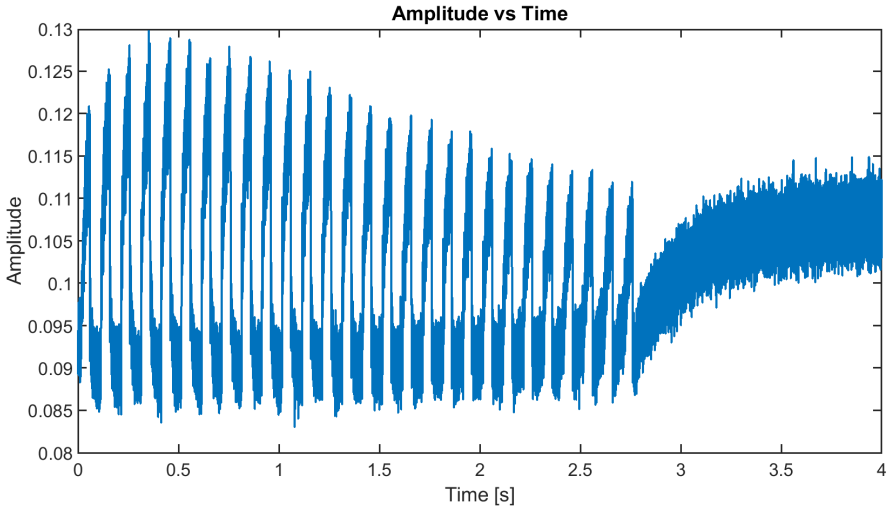

Figure 4.11: Magnitude of a discarded dataset of 15 mW

Why these data exhibit a different trend from others is still unclear to us. We can assume that the data collected for 10 mW and 15 mW differ from one to the other because multiple measurements are taken on the same bead

and the heat is 'trapped' from the environment. Indeed, 6 measurements are made on the same microsphere with the laser 2 for each power. This can lead to overheating of the microsphere which will follow other behaviors. Another reason may be that the agarose around the microsphere, given repeated heating begins to lose its properties.

4.3.2 Beads' behaviors

Implementing an in-depth analysis of our data, we found that they exhibit 2 different behaviors when heated.

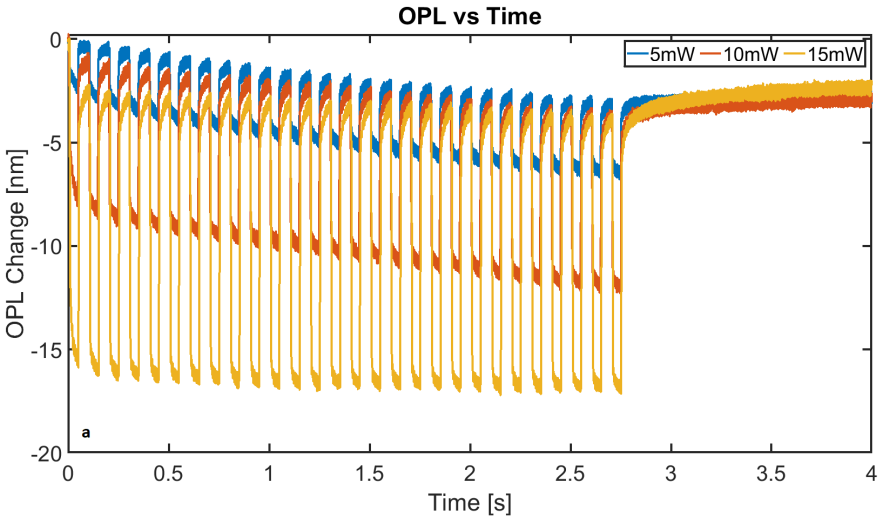

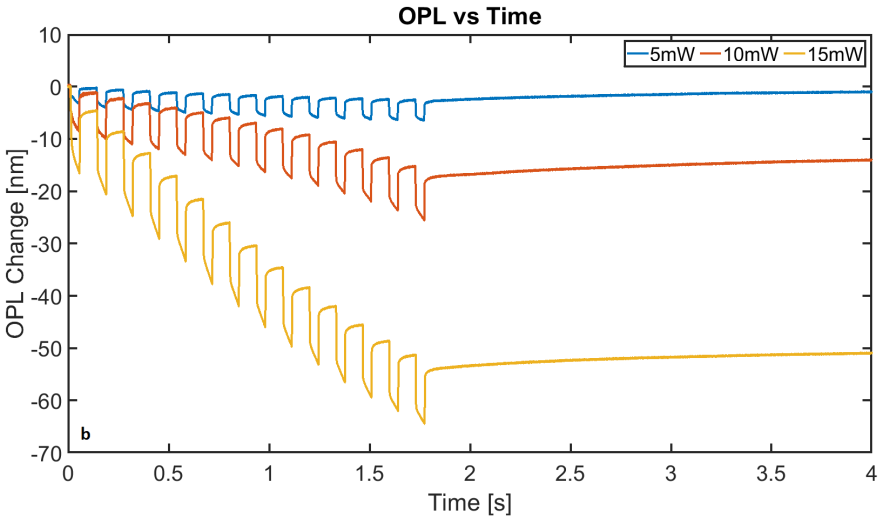

Figure 4.12: Optical path length of two different beads sample exposed to different laser power. (a) Microsphere showing low inelastic creep. (b) Microsphere showing significant creep.

It can be seen that for Figure 4.12a there is no substantive shift of the baseline, while for Figure 4.12b there is an ascertainable shift.
This slow shift is not due to position drift, as this would cause a loss of visibility of the fringes that we do not observe.
We can provisionally attribute this displacement to the inelastic deformation of the sphere heated inhomogeneously by our laser[40]. This depends on the molecular properties of the polymer and the past deformations it has undergone[41] . The strong difference in inelastic behavior could be attributed to a possible different annealing history of the two microspheres.
They are part of the data-set considered valid according to the criteria used. Nevertheless they still show these two different behaviors. In fact, one cannot attribute the base line shift to heating, but as described, to a different behavior intrinsic to the miscrosphere. However, sometimes different behavior was recorded for different laser powers in the same sample. One explanation may fall on sample preparation, which although the usual procedure is

always followed, is still susceptible to human error.

An experiment by moving the z-axis of the sample during measurement was conducted (as explained in the materials and methods section). By moving the knob (of the z-axis) at intervals of 50 nm, it was possible to observe how the baseline also underwent a shift.

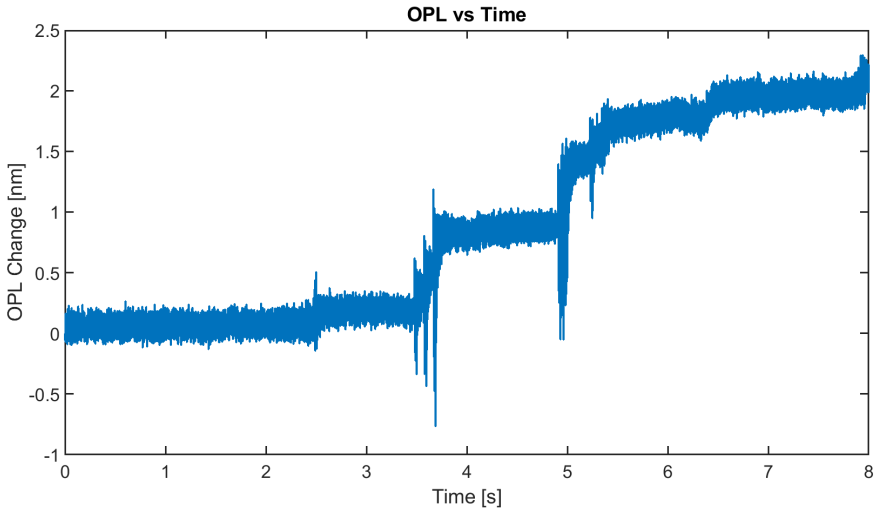

Figure 4.13: Movement of the z-axis during the experiment. No heating was applied in this measurement, but the knob for manual control of the z-axis on the sample was moved during the analysis. The total movement was 300 nm; 6 movements of 50 nm each were made.

The result (appreciable in Figure 4.13) might indicate that this baseline movement may be due to microsphere movement during the measurement. The agarose gel around the microsphere may have lost its immobilizing property due to continuous heating. However, this is only a hypothesis we can make since we have no data to confirm this.

4.3.3 Fresnel model

In order to best understand why a baseline shift occurs and how the change in the reflection affect it, we performed calculations regarding reflection and

how it changes in relation to refractive index and consequently temperature. To so so we invoke the Fresnel equations.
The Fresnel equations describe the behaviour of an electromagnetic wave at a plane surface[42]. It describes the reflection and transmission of light on an interface between two different mediums[43].
The contribution of reflection at the top and bottom of our microsphere will be equal to:

$$R_b = R_t = \frac{|n_2 - n_1|^2}{|n_1 + n_2|^2} = \frac{|1.57 - 1.335|^2}{|1.57 + 1.335|^2} = 6.54 \cdot 10^{-3} \tag{4.2}$$

Where R_t is the reflection at the top and R_b at the bottom of the microsphere. The values of n_1 and n_2 are the refractive indices of agarose and polystyrene, respectively. The result of getting the equation (4.2) is the reflection of the sample, what we are interested in now is the intensity of the amplitude of the interference pattern.

$$I_t = R_t \cdot I_0 \tag{4.3}$$

$$I_b = R_b \cdot (1 - R_b)^2 \cdot I_0 \tag{4.4}$$

Where I_0 is the intensity of our light source, which by convention is set equal to 1.The signal has been normalized so absolute intensity is not important and can be set to 1. Also, we are only interested in relative changes in reflectivity because that is what we can extract from the amplitude data. I_t and I_b are the intensity of the reflection of the light.
Having defined the intensity of the reflection we now have to calculate amplitude of the interference. However, when we talk about interference, we need to know the electric field E. The relationship that governs intensity and magnetic field E is:

$$I = |E|^2 \rightarrow E = \sqrt{I} \tag{4.5}$$

Through the relationship found, we can define and calculate the amplitude of

the interference, i.e the amplitude of the fringes in our measurements, which will be equal to:

$$A = |E_t| \cdot |E_b| \tag{4.6}$$

$$A = \sqrt{I_t} \cdot \sqrt{I_b} \tag{4.7}$$

$$A = \sqrt{R_t \cdot I_0} \cdot \sqrt{R_b \cdot (1 - R_b)^2 \cdot I_0} \tag{4.8}$$

As previously explained I_0 by convention is equal to 1 and R_t and R_b have the same value so the final relationship for the amplitude will be:

$$A = R_b \cdot (1 - R_b) \tag{4.9}$$

Replacing numerically with the values we calculated for R_b, we will have:

$$A = 6.54 \cdot 10^{-3} \cdot (1 - 6.54 \cdot 10^{-3}) = 6.50 \cdot 10^{-3} \tag{4.10}$$

The value just calculated in the equation indicates the magnitude of the interference when there is no laser exposure.
However, we know that when there is laser exposure, the refractive index also changes (equation 3.2), and consequently we will have a change in the amplitude as well. Through the average temperatures calculated for the three different laser powers and relation 3.2, it is possible to estimate the new refractive index for each of these powers.
The values of the refractive index change are tabulated below

	5 mW	**10 mW**	**15 mW**
Δn	$-1.72 \cdot 10^{-4}$	$-4.20 \cdot 10^{-4}$	$-7.74 \cdot 10^{-4}$
n	1.56983	1.56958	1.56923
R	$6.54 \cdot 10^{-3}$	$6.52 \cdot 10^{-3}$	$6.50 \cdot 10^{-3}$
A	$6.49 \cdot 10^{-3}$	$6.48 \cdot 10^{-3}$	$6.4 \cdot 10^{-3}$

Table 4.6: Values of the refractive index change (Δn), refractive index (n), Refraction (R) and amplitude of the interference (A) for each laser power.

Taking the values just calculated for Δn we are going to estimate the refractive index by summing the value of the change in the refractive index. Through the relationships between the estimated reflection (4.2) and the interference's amplitude (4.9), it was possible to calculate first the reflection and then the amplitude with the new reflection indexes.
Taking the amplitude data for different laser powers, we could see that there is a linear decrease in it. This calculation helped us to better understand how as temperature increases there is a decrease in the amplitude of the reflection's interference.

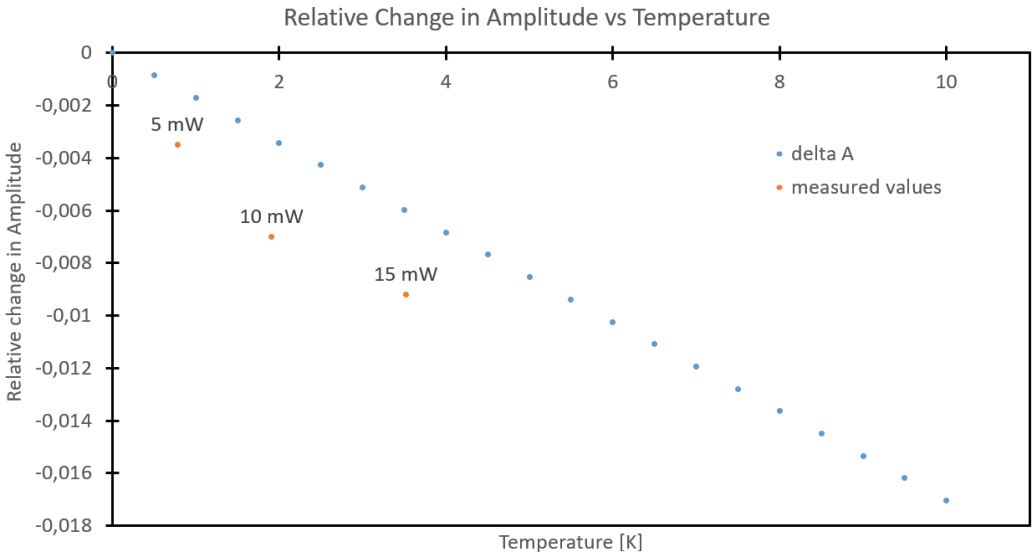

Figure 4.14: Relation between the relative change in amplitude and the temperature.The dotted blue line is the theoretical predction, while the 3 orange dots refer to the measured relative amplitude for the 3 different laser powers.

For the calculation of reflection just performed, we considered the refractive index value for agarose gel found in the literature that is 1.335[44, 45] and constant.

Furthermore, it is reported in the literature that agarose gel maintains its state and gel properties up to a temperature of 50°C[46]. In our experiments these temperatures are not reached, however, a slight deviation of the refractive index cannot be excluded. However, as can be seen from Figure 4.14, the measured values (in orange) differ from the theoretical values (blue dotted line). If we continue horizontally for each measured values we encounter a value from the theoretical graph which indicates the temperature difference to which the sample is subjected. The temperature values we found (Table 4.2) are smaller than those we can find by implementing this estimation. If we move horizontally to identify the value for 5 mW we find that it crosses the line for the temperature value at about 2.8 K. Repeating the same process for 10 mW and 15 mW we find a value around 3.9 K and 5.6 K, respectively.

It can be inferred from the graph that the measured values will differ from those we calculated through our model by a value of ≈ 2. According to the values calculated by our model we are underestimating the actual warming value. This may be due to the fact that in all our assumptions we have ignored the environment surrounding our microsphere, which instead seems to play a key role in the measurements. In fact, agarose could trap heat during experiments, and this could lead to the overheating we estimated earlier and it could be a possible explanation why we see in some sample the baseline shift.

Chapter 5

Conclusions

In this thesis, a study of the thermal expansion of polystyrene beads using optical coherence tomography was performed. The sensitivity found by our set-up allowed us to pick up even the smallest changes in the order of picometres.

The construction of a theoretical model enabled us to lay the foundation for understanding the behaviour of microspheres during laser heating. Using three different laser powers 5 mW, 10 mW, 15 mW, we could see that there is an increase in OPL, as expected.

However, we have been able to ascertain that a change in size lead to a decrease in the refractive index of the polystyrene and consequently a decrease in the amplitude of the refraction. This explains why we saw a negative trend in the OPL and a decrease in amplitude of the interference of the light when the laser is on. We further noticed that, if for 5 mW and 10 mW we obtained reproducible results, they became increasingly chaotic and uneven as the laser power increased.

In addition, we have verified different behaviour in our microspheres when they are heated. If the first case could be related to different things as: sample preparation, change in the proprieties of Agarose during the heating process or other external factor; the latter is due to the inhomogeneous heating and the inelastic creep.

Overall, the optical coherence tomography technique allows minimal changes in the OPL to be measured. However, there are inconsistencies between the theoretical model we created and the actual experimental data. These are dictated by several factors, one of which did not allow us a more in-depth

analysis is the concentration of fluorophores within a single microsphere. This information could lead us to understand the actual heating temperature and thus discern the different behaviours.
It must be emphasised, moreover, that the model we created largely explained the results found experimentally.

Bibliography

[1] Aumann et al. *Optical Coherence Tomography (OCT): Principle and Technical Realization*, pages 59–85. Springer International Publishing, 2019.

[2] A F Fercher et al. Optical coherence tomography - principles and applications. *Reports on Progress in Physics*, 66(2):239, jan 2003.

[3] Edinburgh University. microscopy. https://www.ed.ac.uk/clinical-sciences/edinburgh-imaging/for-patients-study-participants/tell-me-more-about-my-scan/what-is-microscopy.

[4] Glenn Stark. https://www.britannica.com/science/light.

[5] https://ec.europa.eu/health/scientific_committees/opinions_layman/en/energy-saving-lamps/l-3/1-light-electromagnetic-spectrum.htm.

[6] Vanq. Full spectrum of the light. https://www.vanqled.com/how-to-choose-the-best-full-spectrum-led-grow-lights-for-your-crops.

[7] Technology Network. Wide Field Microscopy. https://www.technologynetworks.com/analysis/articles/an-introduction-to-the-light-microscope-light-microscopy-techniques-and-\applications-351924.

[8] Roane et al. *Microscopic Techniques*, pages 157–172. Elsevier Inc., 2009.

[9] Ernst Abbe. Beiträge zur Theorie des Mikroskops und der mikroskopischen Wahrnehmung. *Archiv für mikroskopische Anatomie*, 9:413–418, 1873.

[10] George Biddell Sir Airy. On the diffraction of an object-glass with circular aperture. *SPIE milestone series*, 178:3–11.

[11] Lord Rayleigh F.R.S. XXXI. investigations in optics, with special reference to the spectroscope. *The London, Edinburgh, and Dublin Philosophical Magazine and Journal of Science*, 8(49):261–274, 1879.

[12] Siegfried Weisenburger and Vahid Sandoghdar. Light microscopy: an ongoing contemporary revolution. *Contemporary Physics*, 56(2):123–143, 2015.

[13] Jung et al. Performance of scientific cameras with different sensor types in measuring dynamic processes in fluorescence microscopy. *Microscopy research and technique*, 76,8:835–43, 2013.

[14] Nwaneshiudu et al. Introduction to confocal microscopy. *Journal of Investigative Dermatology*, 132(12):1–5, December 2012.

[15] St Croix et al. Confocal microscopy: comparisons, applications, and problems. *BioTechniques*, 2005.

[16] Swaim W.D. Overview of confocal microscopy. methods in molecular biology (clifton, n.j.). pages 187–201, 2010.

[17] Elliott A. D. Confocal microscopy: Principles and modern practices. 2020.

[18] Scientific Volume Image. Airy's Disk. `https://svi.nl/AiryDisk`.

[19] Gray et al. *Basic confocal microscopy / W. Gray (Jay) Jerome, Robert L. Price, editors.* Springer, Cham, Switzerland, second edition. edition, 2018.

[20] Sanderson et al. Fluorescence microscopy. *Cold Spring Harb Protoc.*, 10, 2014.

[21] Stokes Shift. https://en.wikipedia.org/wiki/Stokes_shift.

[22] Nikon. Fluorescent image. https://www.microscopyu.com/galleries/fluorescence.

[23] Adrian Podoleanu. Optical coherence tomography. *The British journal of radiology*, 78:976–88, 12 2005.

[24] Huang et al. Optical coherence tomography. *Science*, pages 1178–1181, 1991.

[25] Podoleanu A. G. Optical coherence tomography. *Journal of microscopy*, page 209–219, 2012.

[26] Drexler et al. Optical coherence tomography today: Speed, contrast, and multimodality. *Journal of biomedical optics*, 19:71412, 07 2014.

[27] J.F. de Boer et al. Improved signal-to-noise ratio in spectral-domain compared with time-domain optical coherence tomography. *Opt. Lett.*, 28(21):2067–2069, Nov 2003.

[28] Leitgeb et al. Performance of fourier domain vs. time domain optical coherence tomography. *Opt. Express*, 11(8):889–894, Apr 2003.

[29] Asgari et al. Sub-nanometer measurement of transient structural changes in dye-doped polystyrene microspheres. *Opt. Continuum*, 2(2):259–265, Feb 2023.

[30] ThermoFischer. FluoSpheres™ Polystyrene Microspheres, 10 µm, orange fluorescent (540/560), for blood flow determination.

[31] Azooptics. Optical path length. https://www.azooptics.com/Article.aspx?ArticleID=692.

[32] D. Burnett. The relation between refractive index and density. *Mathematical Proceedings of the Cambridge Philosophical Society*, 23(8):907–911, 1927.

[33] He et al. Simultaneous determination of glass transition temperatures of several polymers. *PLOS ONE*, 11:1–12, 03 2016.

[34] Sasabe Hiroyuki and Saito Shogo. Effects of temperature and pressure on the dielectric constant in non-polar polymers. *Polymer Journal*, 1972.

[35] Refractive index permeability relation. `https://en.wikipedia.org/wiki/Refractive-index#Relative-permittivity-and-permeability`.

[36] Nguyen et al. *Why Two Sigma? A Theoretical Justification*, pages 10–22. Springer Berlin Heidelberg, Berlin, Heidelberg, 2003.

[37] T-test. `https://en.wikipedia.org/wiki/Student%27s_t-test`.

[38] Mishra P. et al. Application of student's t-test, analysis of variance, and covariance. ann card anaesth. *PubMed*, pages 407–411, 04 2019.

[39] Understandig the T-test in excel . `https://www.drdawnwright.com/tail-of-the-test-interpreting-excel-data-analysis-t-test-output/`.

[40] Hal F. Brinson and L. Catherine Brinson. *Polymer engineering science and viscoelasticity: An introduction*. 2008.

[41] Lin et al. *Polymer viscoelasticity: basics, molecular theories, experiments, and simulations*. World Scientific, 2011.

[42] M A B Whitaker. Improved treatment of Fresnel equations. *Journal of Physics A: Mathematical and General*, 12(3):297, mar 1979.

[43] Electical. Fresnel equations. `https://www.electrical4u.com/fresnel-equations/`.

[44] Tin-Man Lee et al. Optical characterization of contrast agents for optical coherence tomography. In Darryl J. Bornhop, Ramesh Raghavachari, Samuel I. Achilefu, and Alexander P. Savitsky, editors, *Genetically Engineered and Optical Probes for Biomedical Applications*, volume 4967, pages 129 – 134. International Society for Optics and Photonics, SPIE, 2003.

[45] Fujiwara et al. Agarose-based structured optical fibre. *Scientific Reports*, 10, 04 2020.

[46] Podeă et al. Studies on agaroses; 1. specific refractive index increments in dimethyl sulfoxide and in water at various wavelengths and temperatures. *Polymer*, 36(26):4967–4970, 1995.